ENICO-1011

# TECHNICAL AND ECONOMIC FEASIBILITY OF ZEOLITE ENCAPSULATION FOR KRYPTON -85 STORAGE

September 1979

Idaho Falls, Idaho 83401

EXXON NUCLEAR IDAHO COMPANY, Inc.

Prepared For The
DEPARTMENT OF ENERGY

IDAHO OPERATIONS OFFICE UNDER CONTRACT DE-AC07-79ID01675

ENICO-1011

Distributed Under Category:
UC-70
Nuclear Waste Management

# TECHNICAL AND ECONOMIC FEASIBILITY OF ZEOLITE ENCAPSULATION FOR KRYPTON-85 STORAGE

R. W. Benedict, A. B. Christensen, J. A. Del Debbio
J. H. Keller, and D. A. Knecht

September 1979

EXXON NUCLEAR IDAHO COMPANY, INCORPORATED

PREPARED FOR THE
DEPARTMENT OF ENERGY
IDAHO OPERATIONS OFFICE
UNDER CONTRACT DE-AC07-79IC01675

## ABSTRACT

This report presents experimental results and analyses to demonstrate the technical and economic feasibility of encapsulation by zeolites as a method to immobilize krypton-85 for safe, long-term storage. The process, which is feasible for a reference 2000 metric ton of heavy metal per year reprocessing plant, would encapsulate krypton at approximately 20 $cm^3/g$, using temperatures greater than 575$^{o}$C and pressures greater than 1600 atm. A conceptual design and cost estimate was made for a commercial-scale facility, using well-established technology for building, operating, and containing krypton-85 within such a processing system. Safety considerations to contain any krypton released from the processing equipment are within existing technology.

| Page | Line | Errata |
|---|---|---|
| iv | 5 | Change "1660" to "1600" |
| 17 | 23 | Equation (9) should read: $$V = V_{eq}\left[1-\frac{6}{\pi^2}\sum_{n=1}^{\infty}\frac{1}{n^2}\exp\left(-\frac{Dn^2\pi^2 t}{R_o^2}\right)\right] \quad (9)$$ |
| 18 | 8 | Change "Q" to "$Q_\infty$" |
| 18 | 25 | Change "negative" to "positive" |
| 31 | 1 | Change lable on curve "OD-2 400°C, 1220 atm" to "OD-2 500°C, 1220 atm" |
| 71 | 1 | Replace Figures A-6 and A-7 by the following: |

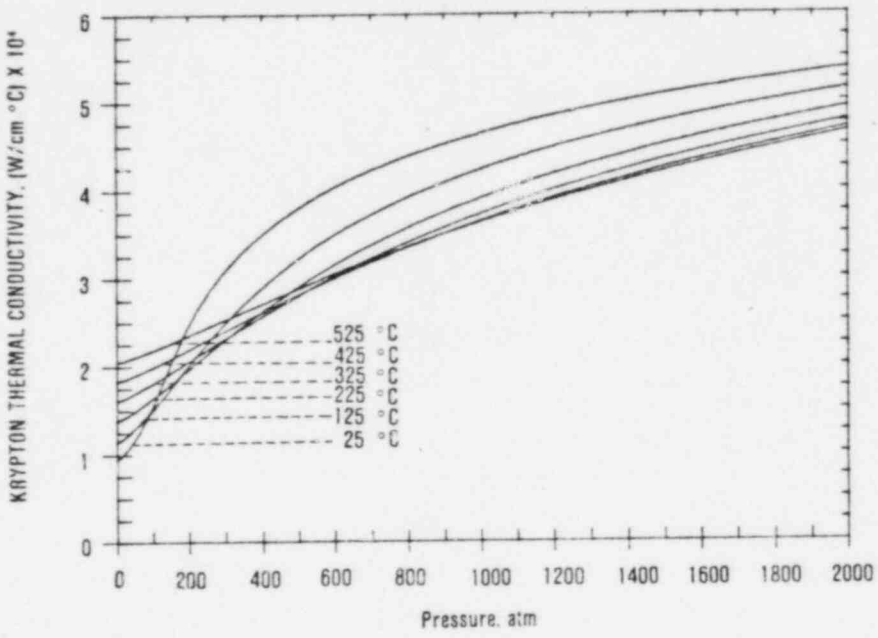


Figure A-6

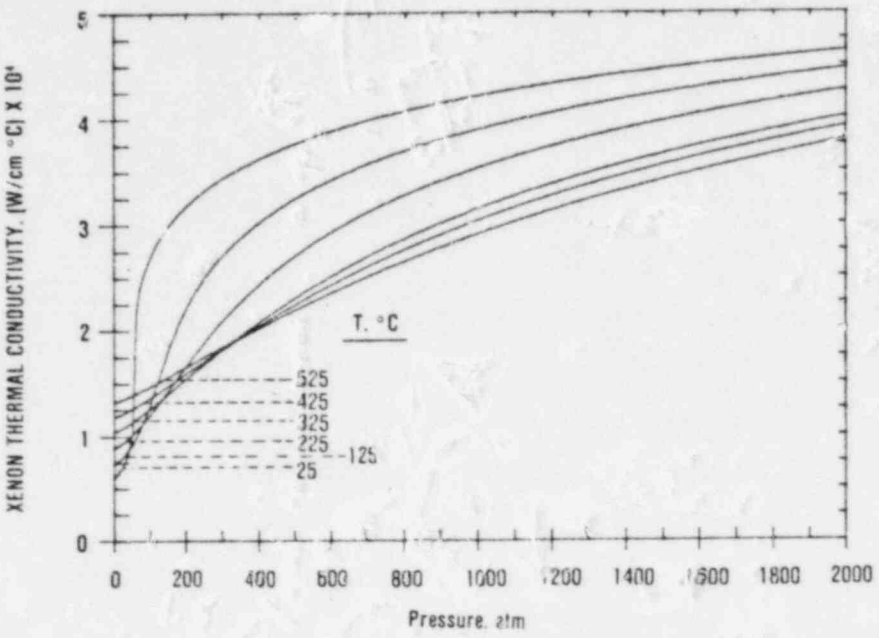
XENON THERMAL CONDUCTIVITY, (W/cm °C) X 10⁴
5
4
3
2
1
0
T, °C
525
425
325
225
125
25
0
200
400
600
800
1000
1200
1400
1600
1800
2000
Pressure, atm

Figure A-7

## SUMMARY

Federal regulations limit the release to the environment of krypton-85 produced by nuclear fission in commercial electric power generation systems. These regulations apply to nuclear fuels irradiated after January 1, 1983. This report presents experimental results and analyses to demonstrate the technical and economic feasibility of encapsulation in zeolites to immobilize krypton-85 for safe, long-term storage.

Encapsulation measurements were made at 400 to 575°C and 1200 to 2000 atm, using pure krypton and mixtures of krypton and xenon that contain up to 64% xenon. Loadings from 20 to 40 $cm^3$ at standard temperature and pressure of krypton per gram of sodalite were obtained. These values provide volumes of immobilized krypton equal to volumes of pressurized krypton at about 16 to 32 atm, respectively. Loadings were higher for leached than for unleached sodalites. Equilibrium krypton loadings were reduced by only about 15% when the xenon content was 50%, with very little xenon (approximately 1 $cm^3/g$) being sorbed.

Krypton leakage measurements were made at 300 to 500°C for short times (about 2 to 24 hours) and at 150°C for long times (about 1 to 12 months). Leakage rates were lower: for unleached versus leached sodalites, for samples with low versus high absorbed water, and for samples with high versus low initial krypton and xenon concentrations. At 150°C, there is evidence that some krypton (approximately less than 0.1% for unleached sodalite) is released rapidly and the rest very slowly. No evidence for crystal damage or increased leakage was observed in a high gamma radiation exposure test (approximately $2 \times 10^9$ rads). For unleached sodalite containing approximately 20 $cm^3/g$ krypton and low amounts of absorbed water, the predicted ten-year leakage at a storage temperature of 150°C was approximately 0.1%, based on leakage measurements carried to one year.

Based on these experimental results, the process that is technically feasible for a reference 2000 metric ton of heavy metal (MTHM) per year reprocessing plant would encapsulate krypton at approximately 20 $cm^3/g$ from krypton at temperatures greater than 575°C and pressures greater than 1660 atm with one batch a day in a 58-L high pressure vessel. Based on preliminary measurements at 500°C, the same process also would be feasible for a 70% krypton and 30% xenon mixture.

A conceptual design and cost estimate was made for a commercial-scale (2000 MTHM per year reprocessing plant) krypton encapsulation facility, operating a 58-L high pressure vessel at one batch a day. Schematics of the facility layout, hot encapsulation system, and a two-gas high pressure vessel are included.

The technology of fabricating, operating, and containing krypton-85 in such a system is well established. A large inventory of krypton-85 will be present in the facility in a lag-storage area and in the high pressure vessel. Safety considerations to provide containment of any krypton released from the processing equipment include conservative design limits on the pressure vessel, a barricade around the high pressure vessel that would contain potential rupture fragments and released gas, and air-tight hot cells. These options are available within existing technology.

Appendices provide detailed information about krypton, xenon, and sodalite properties.

CONTENTS

FIGURES

TABLES

# TECHNICAL AND ECONOMIC FEASIBILITY OF ZEOLITE ENCAPSULATION FOR KRYPTON-85 STORAGE

## I. INTRODUCTION

### 1. Background

Fission of uranium or plutonium produces in moderate yield krypton-85 ($^{85}Kr$), which in the past has been released to the atmosphere. The mobility, chemical inertness, and 10.73-year half-life of this noble gas have lead to a uniform distrib- ution of the released activity in the atmosphere.[1] Options[2] and radiation dose commitment trade-offs[3] for release versus collection and long-term storage of krypton-85 are being evaluated.

Environmental Protection Agency (EPA) regulations will limit the amount of $^{85}Kr$ released to the atmosphere in the U.S. for commercial nuclear fuel irradiated after January 1, 1983. The regulations, entitled "Environmental Protection Standards for Nuclear Power Operations," state that for the entire fuel cycle, operations must be conducted to provide a reasonable assurance that less than 50,000 Ci of $^{85}Kr$ are released to the general environment per gigawatt-year of electrical energy (GWe-yr) produced.[4]

To meet the EPA regulation, the $^{85}Kr$ produced must be collected and stored for sufficient time to allow radioactive decay to reach a level that will allow release consistent with the regulations.[5] This report summarizes the technical and economic feasibility of encapsulation in zeolite, one of the proposed immobilization techniques for the safe storage of $^{85}Kr$.

Two mechanisms in the environment produce $^{85}Kr$: cosmic ray neutron interaction with atmospheric $^{84}Kr$, and spontaneous and induced fission of natural uranium. The steady-state inventories of $^{85}Kr$ produced by these sources have been estimated to be about 12 Ci.[6]

The environmental inventory of $^{85}Kr$ has increased since the inception of manmade fission processes. The three principal sources are weapons testing, plutonium production, and commercial electric power generation.[1]

Atmospheric weapons testing between 1945 and 1962 generated approximately 5 MCi of krypton-85. Atmospheric tests by France and the People's Republic of China since 1962 added more $^{85}Kr$ to the inventory. A larger contribution has been made by plutonium production in the U.S. and other countries. The U.S. plutonium production contributed an estimated 15 MCi to the total atmospheric inventory as of 1966.[7] The worldwide contribution from plutonium production has been estimated to be 38 MCi as of 1970[7] with a continued production of about 1 MCi/yr. The decreased frequency of atmospheric testing and the shift to thermonuclear weapons has decreased the $^{85}Kr$ production rate. The current inventory contribution from these sources is also decreasing due to radioactive decay. Measurements of the $^{85}Kr$ concentration in the atmosphere in 1973 indicated a 53-MCi inventory.[8]

In the U.S. there are currently two facilities processing government-owned spent fuel: the Idaho Chemical Processing Plant (ICPP) and the Savannah River Processing Plant (SRP). In addition, the Hanford (Washington) Purex Plant -- not currently in operation -- has processed spent fuel and released $^{85}Kr$ to the environment. The two operating plants release $^{85}Kr$ to the environment at average rates estimated to be $5.5 \times 10^4$ Ci/yr and $5.7 \times 10^5$ Ci/yr respectively.[9] The ICPP has operated a noble gas recovery facility, which collects a portion of the $^{85}Kr$ produced, on a periodic basis for several years.[10-13] The recovered $^{85}Kr$ is used for research purposes and not stored, so, after various decay periods, this material will enter the environment.

Commerical electric power generation from nuclear-powered, steam/electric facilities is currently the largest source for production of $^{85}Kr$.[1]

Depending on the fuel cycle used in commercial facilities, different quantities of $^{85}Kr$ are produced per metric ton of heavy metal (MTHM) as shown below.[14,15]

TABLE I-I

ESTIMATED AMOUNTS OF KRYPTON-85 PRODUCED FROM DIFFERENT FUELS AND RESULTING EPA RELEASE LIMITS

| Fission Isotope | $^{235}U$, Thermal | $^{239}Pu$, Fast | $^{233}U$, Thermal |
|---|---|---|---|
| Krypton Production ($MCi/GW_e$-Yr) | $\sim$0.3[a] | $\sim$0.2[b] | $\sim$0.6[b] |
| EPA Release Limit (%) | 17 | 25 | 8 |

a. Reference 15.

b. Calculated from fission yields of $^{85}Kr$ (reference 14) for all fuels and $^{85}Kr$ production estimate from reference 15.

Calculations for the light water reactor (LWR) fuel cycle indicate that $3.2 \times 10^5$ Ci of $^{85}Kr$/GWe-yr will be produced.[15]

Thus, the EPA release limits can vary from as much as 25% of the krypton produced by fast fission of plutonium to as little as 8% produced by thermal fission of uranium-233 in a thorium fuel cycle.

In the U.S., installed nuclear generating capacity has reached 52.3 GWe in 72 reactors. An additional 131 reactors are under design, construction, or are planned with a combined capacity 145.6 GWe.[16] The rest of the world has installed capacity of 56.4 GWe with planned additional capacity of 379.7 GWe.[16]

The magnitude of the potential future source of $^{85}Kr$ depends on projections of nuclear generating capacity, which have historically overestimated the installed capacity in the U.S. The draft environmental impact statment on management of commercially generated

radioactive waste uses an installed nuclear generating capacity of 400 GWe by the year 2000 for the U.S. reference case.[15] Though this reference case now may appear to be optimistic, it was used in order not to underestimate the magnitude of the waste management task. Another optimistic capacity is used in the final environmental statement in support of the EPA effluent standards; it uses 1200 GWe installed capacity by 2000 in the cost effectiveness calculations.[17] However, an alternate low-demand scenario given in reference 15 assumes 250 GWe installed capacity by 2000, and appears to be more realistic.

The bulk of the $^{85}Kr$ produced in fission reactors is retained within the fuel elements and less than 1% is released during reactor operation.[1,15] The remainder is available for release or containment during chemical reprocessing or during long-term storage of the spent fuel elements.

No commerical nuclear fuel reprocessing plants are licensed to operate in the U.S. at this time. One facility, the Nuclear Fuel Services plant in West Valley, New York, operated from 1966 to 1972. The $^{85}Kr$ liberated from the processed fuel was released to the atmosphere. A new 1500 metric ton of heavy metal (MTHM) per year plant has been built in Barnwell, South Carolina by Allied-General Nuclear Services but has not received a license to operate. The initial plan was to release the liberated $^{85}Kr$ to the atmosphere; however, space is provided in the plant to install necessary equipment to meet the EPA regulations. No operation is planned at a third plant, built by the General Electric Co., at Morris, Illinois. Exxon Nuclear Company, Incorporated of Richland, Washington, prepared a preliminary safety analysis for a proposed 2100 MTHM per year reprocessing plant.[18] Two conceptual designs and cost estimates of generic commercial reprocessing plants have been issued with respective capacities of 3000[19] and 2000[15] MTHM/yr.

In order to meet the EPA regulations, the $^{85}Kr$ released from the spent fuel during reprocessing will have to be collected and

contained to allow for decay. Greater than 99% of the $^{85}Kr$ is released during fuel shearing and dissolution.[1,15] The released $^{85}Kr$ will be swept from these steps by a dissolver off-gas (DOG) stream. The DOG stream contains the air components of the sweep gas; the gaseous fission products including krypton, xenon, iodine, tritium, and carbon-14; and various chemical species arising from the fuel dissolution.[15]

A comparison of the fission yields of krypton and xenon for the fission of $^{235}U$ by thermal neutrons results in a Xe to Kr ratio of 7 to 1.[14] Depending on the design flow rate of the DOG system, the noble gas concentration will be on the order of hundreds of parts per million. Due to the shift in the mass yield curve with the mass of the fissioning nuclide, the Xe to Kr ratio will be higher for plutonium-239 fission. The resulting expected Xe to Kr ratio will be about 9 to 1 for the LWR uranium fuel cycle. Other fuel cycles, whether plutonium or liquid metal fast breeder reactor (LMFBR), will result in different Xe to Kr ratios.

Any economic scenario for the containment of the $^{85}Kr$ requires the separation of the noble gases from the bulk of the DOG flow. There are several potential methods for this separation.[1,5,10-13,15,18-23] However, only cryogenic distillation has been used on a large scale.[5,10-13,20,21] Two other processes, diffusion through permselective membranes[22] and absorption by fluorocarbon solvents,[23] have been tested on bench and pilot scales respectively.

As a result of the extensive experience with cryogenic distillation in the air products industry, the intermittent operation of a small unit at the ICPP,[10-13] and the commercial availability of systems for reprocessing plants, the cryogenic distillation process was selected as the reference system in the draft environmental impact statement on commercial waste management.[15,24] A commercial cryogenic $^{85}Kr$ separation system is also being installed on a Japanese reprocessing plant at Tokai. This facility has a 215 MTHM/yr rate,

making it smaller than the reference reprocessing plant in the U.S. An $^{85}Kr$ decontamination factor near 1000 is expected; the design Kr product purity is 90% with argon being the major impurity.

The fluorocarbon absorption system is undergoing pilot plant scale testing at Oak Ridge Gaseous Diffusion Plant[23] and is the reference process chosen for the conceptual design of a 3000 MTHM per year plant.[19] This concept appears capable of achieving the desired separation of the fission product noble gases from the DOG stream and may not require as extensive feed gas pretreatment as that required in the cryogenic systems. In test runs without Xe present, Kr product purities of 50 to 80% were obtained. When Xe is present in the feed stream, the product normally contains Xe as the major fraction. Testing involving chromatrographic separation or possible cryogenic distillation is underway to purify the product stream further. However, an unresolved issue concerns the presence of impurities in the product stream. Fluorine- and chlorine-containing impurities could have a serious effect in the storage containers.[25]

Once separated from the DOG stream the $^{85}Kr$ will have to be stored in a safe manner for 50 or more years to meet the EPA regulations.[5,15,18-21,24,26,27] Krypton can be stored in two general forms: gaseous[5,15,18-20,24,27] or solid.[26] Figure I-1 illustrates these options for the case of physical immobilization: approximately $10^{25}$ atoms of krypton can be stored in one large container, or one Kr atom can be stored in each of about $10^{25}$ atomic-sized containers.

The approximate annual volumes of immoblized krypton required for a 2000 MTHM per year reprocessing plant are shown in Table I-I for three of the storage options.[26] All volumes lie within approximately a factor of ten and none of the processes can be ruled out on this basis.

The reference containment technique chosen for inclusion in the draft environmental inpact statement on commercial waste management is storage in pressurized gas cylinders. An evaluation of this method[27] and the results of corrosion screening tests of the decay product

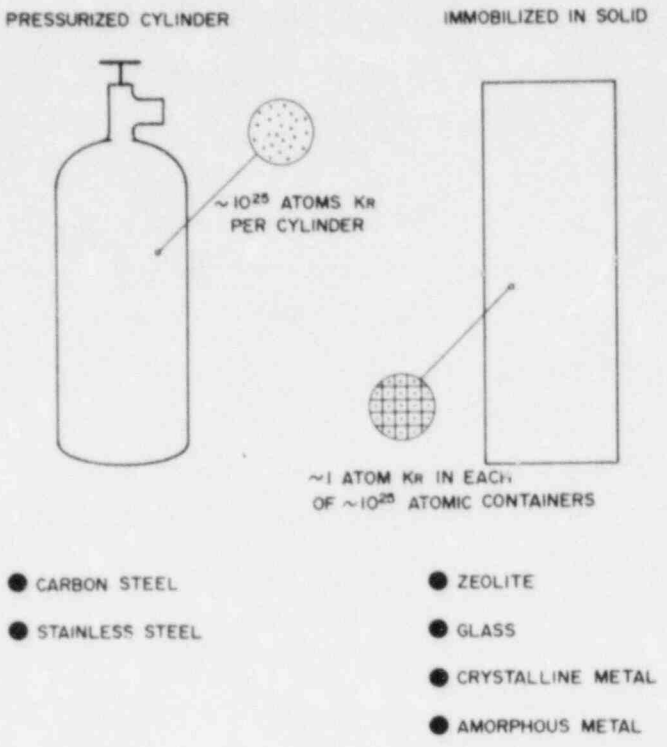


Figure I-1. Options for storing Krypton-85: as a gas or immobilized in a solid.

TABLE I-II

ANNUAL REQUIREMENTS OF MATERIALS USED TO IMMOBILIZE $^{85}Kr$ FOR A 2000 MTHM PER YEAR REPROCESSING PLANT[26]

| Material | Annual Volume, $m^3$ |
|---|---|
| Pressurized Cylinders (34 atm) | 7 |
| Sodalite | 7 - 14 |
| Sputtered Metal | 0.8 - 2 |

a. Annual production is assumed to be 17 MCi or 190 $m^3$ at 0°C and 1 atmosphere of 6% $^{85}Kr$ in krypton.

rubidium[28] have been published. The potential for leakage and release of the $^{85}Kr$ from failed high pressure cylinders and the necessity for heat removal requires that an expensive krypton storage facility (KSF) be used.[15,19,24]

Increased safety would result if the $^{85}Kr$ were immobilized in a solid form rather than as a gas in pressurized cylinders. An evaluation of several immobilization methods was made.[26] The methods evaluated included: high-temperature, high-pressure sorbtion in zeolites, glass, metal, and other solids; ion implantation/sputtering in solids;[29,30] and low-temperature metal vapor deposition. The most promising methods appeared to be sorption in zeolites or ion implantation/sputtering in amorphous metals.

If the $^{85}Kr$ is contained in a solid by one of the above techniques, the solid produced must be further transferred or packaged for storage for the required decay period.[31] An evaluation of possible techniques to prevent dispersal of the $^{85}Kr$-contaminated solids during handling, transport, and storage was made.[32] Several potential methods of immobilizing solids were considered: glass, metal, and polymer matrices; pressed (isostatic) matrices; cement blocks; bitumen blocks; and porous metal containers. Several methods were eliminated because of high process temperature requirements or poor radiation stability of the materials. A preferred method was not chosen.

Chemical compounds of the noble gases have been reported, mostly of xenon.[33] Many of the noble gas compounds are compounds of fluorine and are unstable to heat and moisture. Potential decomposition would result in corrosive products not suitable for long-term storage.

Krypton can be converted to a solid material, although not a true compound, by being included in a crystalline cage of host molecules such as water, hydroquinone, and phenol during crystallization. These materials are termed clathrates.[34] However, these bondings are weak and the solids have low decomposition temperatures, precluding serious consideration as storage media for $^{85}Kr$.[34]

Solid adsorbents, which interact with noble gases, offer the potential for holding the gases in solid form if the energy of the interaction is strong enough to prevent easy loss or leakage from the

adsorbent.[1,21] Inorganic materials (charcoal, silica gel, and alumina) are capable of adsorbing large quantities of krypton, but the sorbed gas is released easily unless the temperature of the material is maintained at a reduced level. Decay heat produced by $^{85}Kr$ and the potential for loss of refrigeration, with rapid release of sorbed gas, makes the material unattractive for long-term storage.

Zeolites or molecular sieves -- a term designating the adsorption or exclusion of molecules according to size -- offer an attractive potential for sorption and retention of noble gases in general and krypton in particular. Initial investigations of sorption of gases by zeolites were conducted on naturally occurring zeolite minerals. The ability of natural zeolites to adsorb large quantities of guest molecules in place of water was known before 1932 when the early treatment of physical sorption was presented.[35] Barrer classified natural zeolites into three groups based on the ability to adsorb or exclude molecule species depending on size in 1945.[36] These three groups, later expanded to five, defined the approximate dimensions of the molecule channels in the various zeolites.[37,38]

The open molecule channels or pores of fixed sizes normally exclude sorbed molecules larger than a given size in a given zeolite.[37,38] However, certain zeolites, e.g. zeolite A, will adsorb quantities of gases at 350°C and 2000-4000 atm that would normally be excluded at room temperature by the molecule sieves effect, and the adsorbed gases are locked in the zeolite when quenched to room temperatures.[37-40] Barrer and Vaughan established that another zeolite, basic sodalite, would encapsulate krypton at high temperatures (440°C) and high pressure (approximately 1000 atm).[41]

## 2. Purpose and Overview

This report presents the theoretical background and experimental results to support the technical feasibility of encapsulating $^{85}Kr$ in sodalite for long-term storage. Sodalite sorbs krypton from pure krypton or a krypton-xenon mixture at high temperatures and pressures.

The resulting encapsulated product is stable under radiation conditions and will leak less than 0.1% of the encapsulated krypton at 150°C and 10 years.

A preliminary design and cost estimate of a production-scale facility, using commercially available equipment, is shown to support the economic feasibility of the encapsulation process. Special design considerations can reduce potential safety problems.

Appendices give detailed information about krypton-xenon properties and zeolite material characterization.

# II. TECHNICAL FEASIBILITY

## 1. Introduction

Encapsulation and leakage tests of krypton in zeolites were made to evaluate process feasibility. Some specific objectives for the tests were:

(1) Screen materials for krypton trapping ability and leakage in order to specify those most suitable for long-term krypton storage.

(2) Determine the effects of temperature, krypton pressure, encapsulation time, gas composition, and properties for the most promising materials.

(3) Develop models and simulate krypton loadings and leakage at different experimental conditions.

This section presents the background, theory, and experimental results obtained at the INEL for the encapsulation and leakage of krypton and krypton-xenon mixtures in various sorbents.

### 1.1 Background

Initial interest in noble gas encapsulation centered on developing the $^{40}K$ - $^{40}Ar$ method for age determination in minerals using trapped argon.[42,43] Encapsulation of argon, krypton, and other gases in potassium-exchanged zeolite A was reported in a patent.[37,39] In addition, Vaughan and Barrer et al. published studies about helium, argon, and krypton encapsulation in zeolites and crystalline silicas.[41,44-47] And, in recent work, hydrogen was encapsulated in cesium-exchanged zeolite at about 400°C and 885 atm.[40]

Barrer and Vaughan's study of the encapsulation of krypton and argon in sodalite appeared to be the most directly applicable to long-term storage of krypton-85.[41,44] Figure II-1 shows the structural

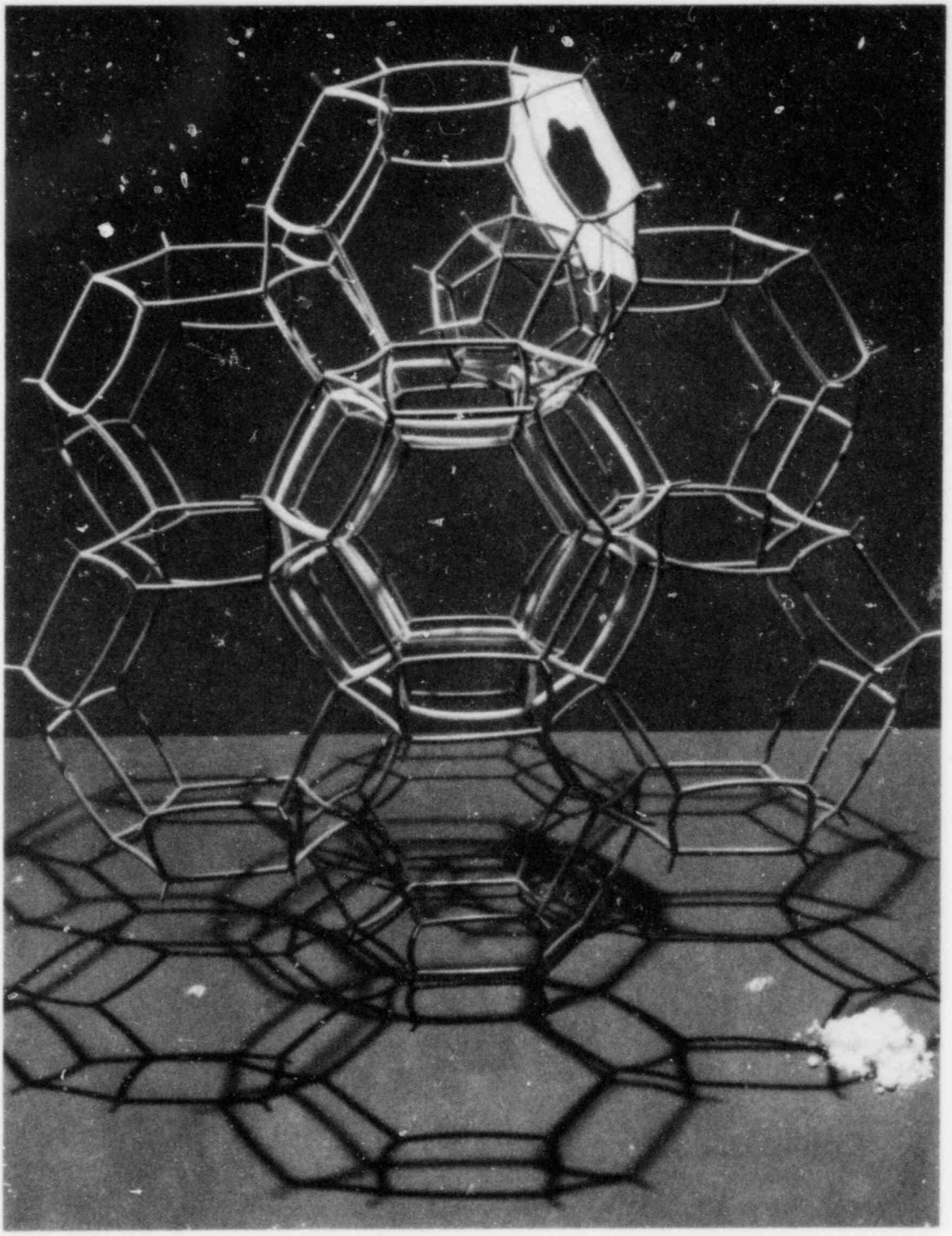

Figure II-1. Model of Sodalite Cages. Upper cage contains a krypton atom. Relative cage opening shown on right side of upper cage.

model of sodalite with one cage (approximately 6.6A free diameter and 2.3A cage opening) containing about a 3.5A-diameter krypton atom (Appendix B gives more detail of the composition). Isotherms of encapsulation loadings at about 400 to 560°C shown in Figure II-2 gave loadings in the range 20-35 $cm^3$ STP/g. If each cage was occupied, a theoretical saturated loading, $V_s$, of 53 $cm^3$ STP of krypton per gram of sodalite can be calculated. Gas release rates (Figure II-3) at about 400 to 560°C could be used to predict low leakage at storage temperatures of about 150°C. Diffusivities were calculated from the leakage rates and were found to depend on 1/T in an exponential manner (Figure II-4). Diffusivity was also affected by the amount of intercalated sodium hydroxide that was in the sodalite. As more excess NaOH was present, the rate of diffusion and leakage decreased.

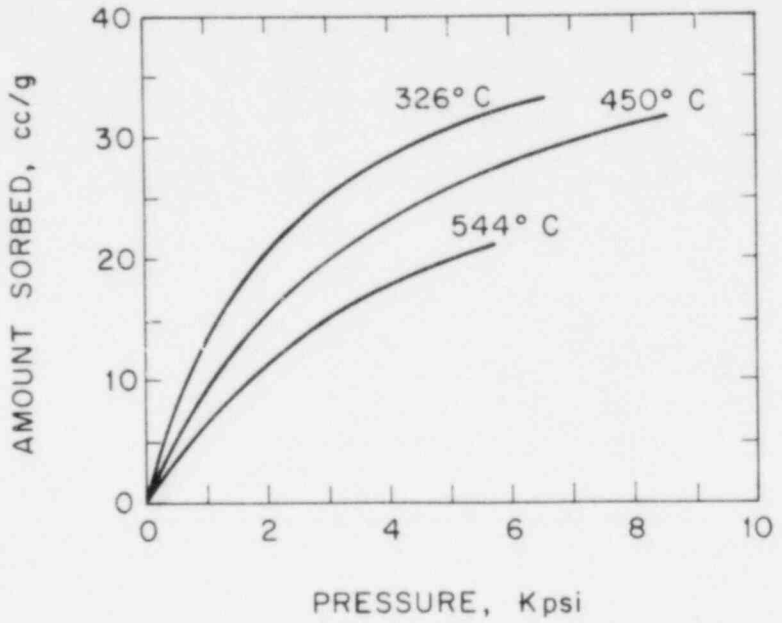


Figure II-2. Isotherms of krypton sorbed on leached sodalite.

Using Vaughan's leakage measurement data at higher temperatures, the release of original krypton and $^{85}Kr$ inventory can be predicted[48] as a function of time at a storage temperature of 150°C, shown in Figure II-5. The straight line, $^{85}Kr$ Decay, shows the fractional depletion of $^{85}Kr$ by radioactive decay and is a measure of the fraction of original $^{85}Kr$ remaining at any time in a storage cylinder

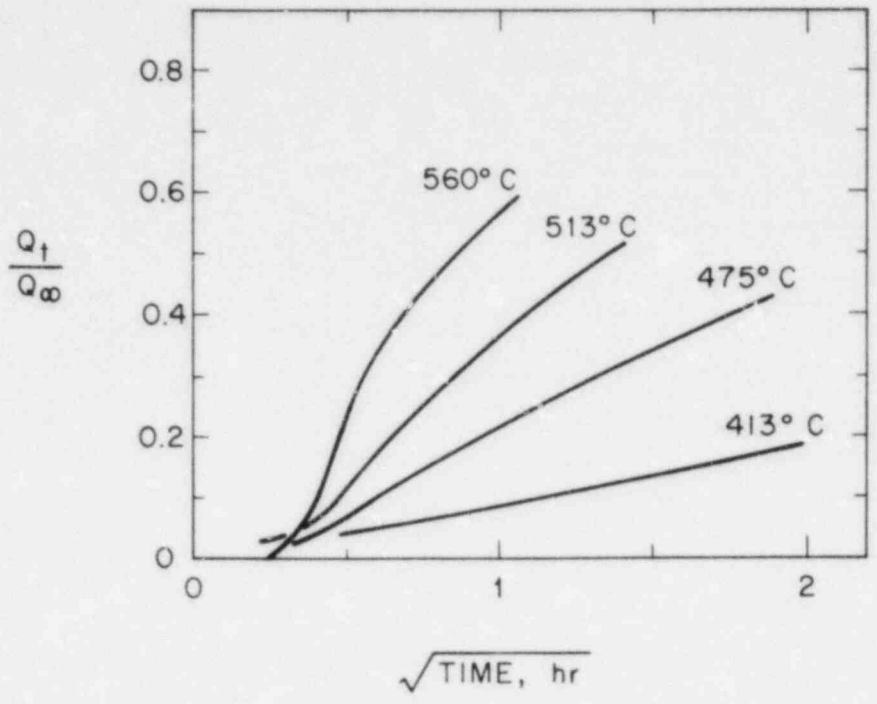


Figure II-3. Rate of fractional leakage from leached sodalite.

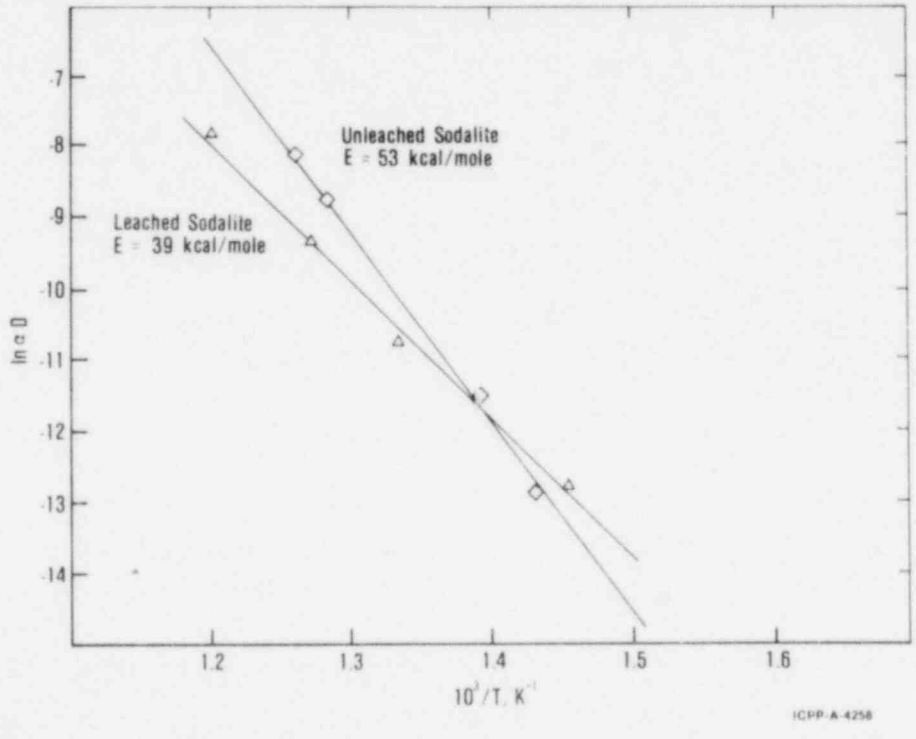


Figure II-4. Temperature dependence of diffusion of krypton in leached sodalite. See Equation (13) for $\alpha$.

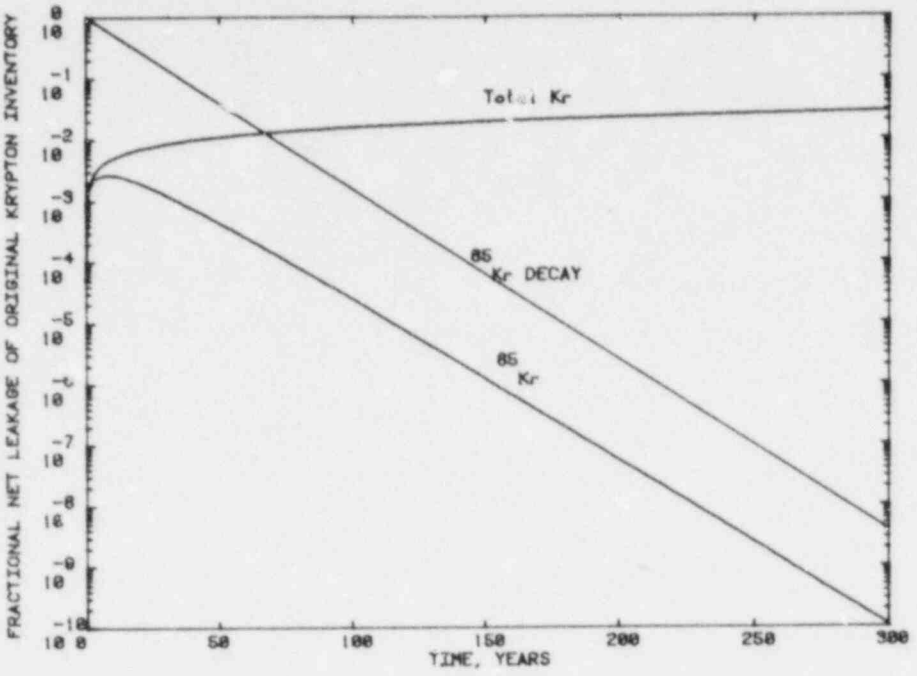


Figure II-5. Calculated release of original krypton inventory from leached sodalite at 150°C as a function of time.

containing either pressurized or encapsulated $^{85}Kr$. The $^{85}Kr$ curve gives the fraction of $^{85}Kr$ which has leaked out of sodalite at any time, but is still contained in the storage cylinder.

Thus, the fraction of $^{85}Kr$ originally stored which could be released at any time due to rupture of a storage container can be determined from the $^{85}Kr$ line for a cylinder containing krypton encapsulated in sodalite. As an example, at approximately eight years, the leakage potential of a damaged storage container represents a safety factor of ~200 for sodalite encapsulation relative to pressurized tank storage.

Encapsulation loading and leakage are a function of temperature, pressure, time, and material characteristics. The amount of krypton encapsulated depends on the equilibrium amount that can be sorbed and on the rate of sorption.

## 1.2 Theory

Typical equilibrium krypton sorption by sodalite is shown by the isotherms in Figure II-2, where sorption increases with the pressure, but decreases with temperature. A Langmuir adsorption model describes this behavior, where a finite number of sorption sites exist and each site can sorb just one atom of krypton.[49] For sodalite, each cage is such a site.

The general form of the Langmuir equation is

$$V_{eq} = \frac{V_s \cdot k(T) \cdot f(p,T)}{1 + k(T) \cdot f(p,T)} \qquad (1)$$

where $V_{eq}$ and $V_s$ are the functional and saturated loadings respectively, f is the fugacity, and k is the equilibrium constant and is a function dependent on the absolute temperature, shown in Equation (2)

$$k(T) = \exp\left[\frac{H}{RT} + \frac{S}{R}\right] \qquad (2)$$

where H and S are the enthalpy and entropy of encapsulation respectively, and R is the universal gas constant.

The rate of encapsulation, which increases with temperature and pressure, depends on the rate of krypton diffusion throughout the zeolite network. Krypton diffusion through the sodalite pores can be described by Fick's law, which describes the change of krypton concentration with time and radial position, r, in the crystal as a function of the concentration.[50-52]

$$\frac{\partial c}{\partial t} = \nabla \cdot D \nabla c \qquad (3)$$

where c is the krypton concentration, t is the time, and D is the diffusion coefficient, or diffusivity. Assuming each zeolite crystal to be a sphere of radius $R_o$, with diffusion in a radial direction only, then Equation (3) reduces to

$$\frac{\partial c}{\partial t} = \frac{1}{r^2}\frac{\partial}{\partial r}\left[ r^2 D \frac{\partial c}{\partial r} \right] \qquad (4)$$

If the diffusion coefficient is assumed to be independent of r and c, then

$$\frac{\partial c}{\partial t} = D\left[\frac{\partial^2 c}{\partial r^2} + \frac{2}{r}\frac{\partial c}{\partial r}\right] \qquad (5)$$

Since D can be assumed constant over a small range of c, Equation (5) can be used to give a rate of encapsulation by assuming the following initial and boundary conditions:[38,50-52]

$$\text{At} \quad t = 0, \; c = 0 \qquad (6)$$

$$\text{At} \quad r = 0, \; \frac{\partial c}{\partial r} = 0 \qquad (7)$$

$$\text{At} \quad r = R_o, c = V_{eq} \qquad (8)$$

The conditions assume that no krypton is inside the zeolite crystal before encapsulation, and that krypton sorption at the crystal-gas interface at $r=R_o$ is always in equilibrium with the gas phase. Therefore, the interface sorption, $V_{eq}$, is a function of the temperature and pressure of the gas phase only as shown in Equation (1).

Under existing experimental conditions, it is not possible to measure the concentration at a given position, r, in the crystal. The average concentration, V, is measurable and can be obtained by integrating c over the crystal volume.

The solution to Equations (3) through (8) describes the loading of krypton in sodalite as a function of time and is shown in Equation (9). Equation (9) may be used to estimate the diffusivity of krypton in sodalite at the conditions used during encapsulation.

$$V = V_{eq}\left[1 - \frac{6}{\pi^2}\sum_{n=1}^{\infty} \exp\left(\frac{-Dn^2\pi^2 t}{R_o^2}\right)\right] \qquad (9)$$

Equation (5) also describes the process of krypton leakage out of the sodalite cages.[38,50,52-55] The initial and boundary conditions shown in Equations (10) and (11) can be used to obtain the solution in Equation (12)

$$\text{At } t=0,\ c=V \text{ For } 0 \le r \le R_o \tag{10}$$

$$\text{At } r=R_o, c=0 \text{ For } t>0 \tag{11}$$

$$\frac{Q_t}{Q_\infty} = 6\left(\frac{Dt}{R_o^2}\right)^{1/2}\left[\pi^{-1/2} + 2\sum_{n=1}^{\infty} \text{ierfc}\left[\frac{nR_o}{(Dt)^{1/2}}\right]\right] - \frac{3Dt}{R_o^2} \tag{12}$$

where $Q_t$ is the volume of gas released at time t, $Q_\infty$ is the volume released at infinite time, $R_o$ is the crystal radius, D is the diffusivity, and ierfc is a mathematical function. For short times and fractional leakage less than 0.3, Equation (12) reduces to Equation (13) where $\alpha$ is a constant for each material.

$$\frac{d\left(\frac{Q_t}{Q_\infty}\right)^2}{dt} = \frac{36D}{\pi R_o^2} = \alpha D \text{ For } \frac{Q_t}{Q_\infty} < 0.3 \tag{13}$$

By measuring the fractional leakage at high temperatures as a function of the square root of time, the diffusivities for krypton leakage can be obtained using Equation (13).

The diffusivity is a strong function of temperature. A krypton atom is held by the repulsive energy between it and the sodalite cage. As the temperature increases, the vibrational energy of a krypton atom in the cage increases until it is larger than the repulsive energy and the krypton diffuses out of the cage. This energy level is called the activation energy E, which is related to diffusivity by Equation (14)

$$D = D_o \exp\left(\frac{-E}{RT}\right) \tag{14}$$

Where T is the absolute temperature, R is the universal gas constant, and $D_o$ is a constant. The energy of activation is always negative, and D varies from 0 to $D_o$ as the temperature increases.

## 1.3 Krypton Diffusivity Behavior

The diffusivity of krypton in sodalite or other sorbents increases with temperature and pressure and depends on the following:

- Sodalite or other sorbent properties
  - (1) Pore channel geometry and dimensions
  - (2) Cation (e.g., sodium) disposition, size, charge, and concentration
  - (3) Adsorbed water content
  - (4) Crystal particle size, typically in the μm range
  - (5) Crystal structural damage
- Sorbed gas (Ar, Kr, Xe) properties
  - (1) Concentration in sodalite
  - (2) Shape, size, and polarity.

### 1.3.1 Sorbent Properties

The pore volume is important for the total capacity but does not affect the desorption rate. The free aperture opening has been shown that as it increases, the activation energy decreases.[56,57] By measuring activation energies, the containment ability of some zeolites can be estimated.

Cations, which can be either part of the structure or intercalated, can influence the desorption process. If a small structural ion is exchanged with a larger ion, the aperture to a cage can be

blocked.[58,59] Changes in molecular sieve properties of zeolites have been shown to occur over the range 26 to 67% ion exchange.[60] The amount of intercalated NaOH in sodalite has also been shown to affect the gas diffusion.[41] By removing the excess NaOH, the activation energies were decreased. Thus, sodalite with suitable amounts of exchanged or added cations could provide low leakage rates for long-term krypton storage.

Adsorbed water affects the rate of krypton diffusion in sodalite. During the encapsulation process, the zeolite is dehydrated to allow rapid krypton diffusion. Previous work has shown that if the crystals are allowed to partially rehydrate at the surface, sorbate trapping was improved.[46] This improvement was postulated to occur because the water blocks the zeolite cage openings. For heulandite and mordenite the surface rehydration was only effective to 100°C, because the surface water is either removed or becomes more mobile.[45] Other work has shown that the heulandite lattice is sensitive to small changes in water content so that intracrystalline water could cause an alumina silicate lattice to expand.[61,62] Both the lattice expansion and heat of water sorption (about 14 kcal/mole) would tend to increase the diffusion of a trapped gas molecule. Since adsorbed water can have a beneficial or a deleterious effect on krypton leakage, it needs to be studied.

Since krypton diffusion in sodalite involves activated jumps from one cage to the next, the number of cages that krypton must go through is an important variable. This quantity is proportional to the crystal radius, $R_o$. Previous work has shown that different size crystals had substantially different sorption and diffusion characteristics.[63] Brandt and Rudlott observed that diffusivity decreased with decreasing particle radius.[64,65] Structural damage in the crystal would decrease effective crystal radius, resulting in more rapid diffusion. Since long-term storage requires stringent restraints for diffusion, the optimum particle size and crystal integrity needs to be known.

### 1.3.2 Sorbed Gas Properties

Previous work has shown that diffusivities during loading and leakage conditions are not always the same, and are dependent on sorbate concentration.[38,63,66] Satterfield and Frabetti observed that diffusivity decreased with increasing sorbate concentration, possibly because of molecule-molecule blockage effects.[63] A model that accounts for the probability of an adjacent cage being occupied also indicates the same behavior when it is not possible for two gas molecules to occupy the same cage.[67] If two krypton atoms cannot occupy a sodalite cage, this type of diffusion would be expected.

For the different rare gases, as molecular diameter increases, the diffusion rate decreases.[41,46,55] For binary gas mixtures, the slower diffusing species have been shown to lower the diffusion rate of the other gas.[63] This interaction would enable a reduction in desorption by operating with a gas mixture.

If the concentration dependence of D is significant, a more convenient parameter for the correlation of the diffusivity by the expression[68]

$$D = \frac{RT}{K} \frac{d \ln p}{d \ln c} \qquad (15)$$

Equation (15) has been shown to be effective for sorption data; however, it would have to be modified for desorption.

## 2. Experimental Procedure

### 2.1 Encapsulation Process Description

The process for encapsulating krypton is shown as a schematic in Figure II-6. The equipment includes a heated pressure vessel, two compressors in series, vacuum pump, accumulator, krypton storage cylinders, a safety vent tank, control gauges, and protective equipment to prevent overpressurization. All gases were recycled to reduce operating costs.

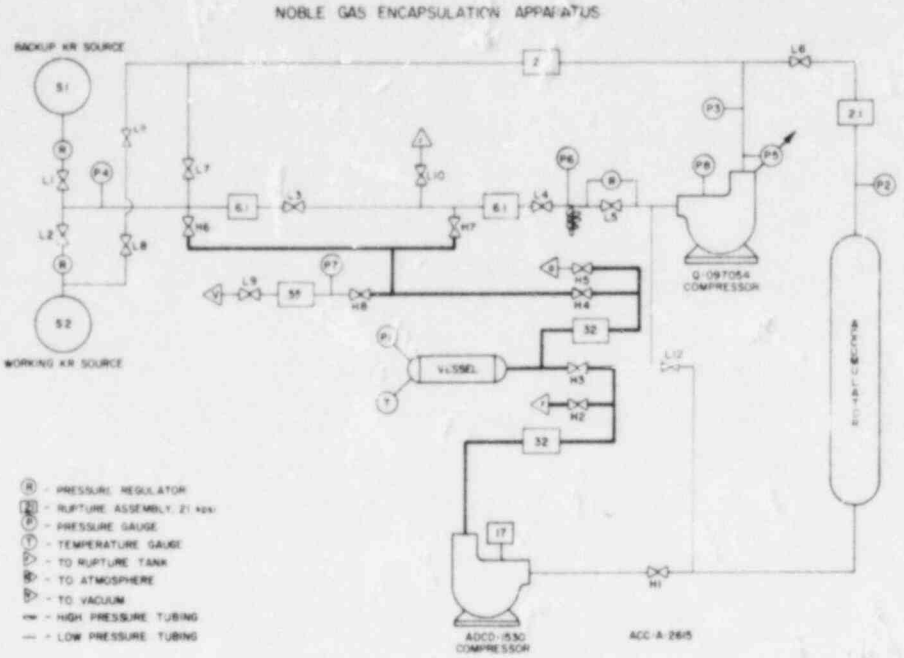


Figure II-6. Schematic of high pressure laboratory-scale system for krypton encapsulation studies.

Pressure Products Industries of Warminster, Pennsylvania, built the equipment. The major components include:

(1) A pressure vessel was made of A-286 stainless steel with a 0.25-L volume. External heating (208 V, 1.5 kW) achieves temperatures of up to 600°C. Maximum temperatures and pressures allowed at levels of constant stress were calculated as 585°C at 1840 atm and 595°C at 1640 atm. Most experiments were made up to 500°C and 1910 atm.

(2) Both compressors are diaphragm types. Compressor Q-097054 is electrically driven and operates at a suction pressure of ~2 atm and a discharge pressure of ~136 atm. Compressor ADCD-1530 is driven by ≤7 atm air pressure and operates at a suction pressure of ~100 to 136 atm and a discharge pressure of ≤2000 atm.

(3) A steel-walled, six-foot-cube barricade built at the INEL houses the apparatus. Plywood and fire-resistant styrofoam lines the inside walls to provide protection against any projectiles. Personnel entry to the barricade is restricted when pressures exceed 340 atm.

(4) Instruments. Temperatures are measured in the pressure vessel using a digital indicator and a type J thermocouple inside a type 316 stainless steel sheath which protrudes into the vessel. Temperatures in the vessel are controlled to ±1% with a Love Model 49 analog set-point proportional controller. High pressures are measured at an accuracy of ±~1% using a Daytronic Model 870 strain gauge and a digital display. Pressure and temperature gauges were calibrated by an on-site calibrations laboratory operated by EG&G.

Quantities of sample (about 0.5 to 80 g) were weighed into porous metal tubes with steel screw-on caps and activated by baking the samples overnight at 400°C under a vacuum of approximately $10^{-4}$ atm. After activation, the samples are weighed inside a dry glove box and transferred to the pressure vessel. Up to 20 tubes could be placed into the vessel at once.

The vessel is heated overnight to the run temperature (T) while under vacuum. At the start of the run, krypton gas from cylinder S2 is pumped into the vessel, using both compressors, until the run pressure (P) is reached, and the pump-up time is recorded. After the run time is reached, the vessel is cooled using a water-air mixture while holding the pressure constant with compressor ADCD-1530. Typical cooling times to 100°C are ~20 minutes from 500°C and ~15 minutes from 400°C. When ambient temperature is reached inside the vessel, most of the gas is vented into S2 and the rest is pumped out by compressor Q-097054.

Chart readings are taken of both vessel temperature and pressure. There is an initial temperature rise of ~1.5% at 500°C and ~5% at 400°C due to compression heating of the gas. Temperature-pressure oscillations (± ~1%) are a result of the time lag in the temperature control system.

The vessel is opened and the samples are placed into the dry glove box. Each tube is weighed and then emptied into labeled, air-tight, glass sample bottles.

## 2.2 Leakage Measurement Process Description

Krypton leakage measurements were made using two different methods, one at high temperatures (about 300 to 500°C, Figure II-7A) and the other at low temperatures (about 50 to 300°C, Figure II-7B).

2.2.1 High Temperature Method (300-500°C). A sample of sodalite loaded with krypton is placed in a quartz tube and evacuated. The tube is then placed inside a tube-furnace at a constant temperature

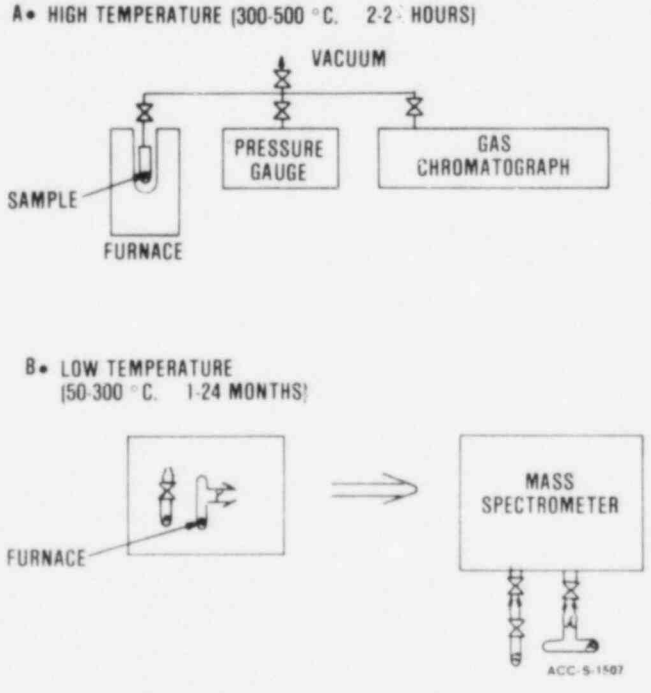


Figure II-7. Schematic of krypton leakage measurement system.
A. High temperature method.
B. Long-term storage method at low temperature.

between 300 to 500°C and the rate of gas evolution is measured by a quartz spiral pressure gauge (Texas Instruments). Periodic gas chromatographic measurements yield the amount of krypton in the evolved gas using a Model 5830A from Hewlett-Packard. Water vapor is continuously trapped at -80°C. Typically 10 to 30% leakage is observed during the 2-5 h krypton evolution rate experiment.

2.2.2 Long-Term Storage Method (50 to 300°C). Zeolite samples loaded with krypton are placed in quartz tubes, and the tubes are evacuated and sealed under vacuum. These are placed in ovens at a constant temperature between 50 to 300°C for a period of days to months. At the end of the test contents of the tubes are analyzed for kypton using a mass spectrometer. Water vapor released from sodalite is not trapped during the test, but can interact with the zeolite in the evacuated tube. The mass spectrometer can also be used to estimate the water vapor present at the end of the test.

## 3. Results and Discussion

### 3.1 Equilibrium Loading

Equilibrium loading of krypton on sodalite was measured at larger pressures (about 1910 atm) than in the previous work. The data obtained at the INEL for leached sodalite SD-LG (see Appendix B for materials designation) is shown with Vaughan's data[44] for his leached sodalite in Figure II-8. The lines represent a fit of the combined results of INEL and Vaughan using the Langmuir sorption model with the parameters $V_s$ used in Equation (1) and H/R and S/R used in Equation (2):

| Source | $V_s$, $cm^3/g$ | H/R, K | S/R |
|---|---|---|---|
| Vaughan[44] | 45.0 | 2103.1 | -8.56 |
| INEL | 44.5 | 2019.5 | -8.25 |
| Combined | 45.2 | 2083.7 | -8.54 |

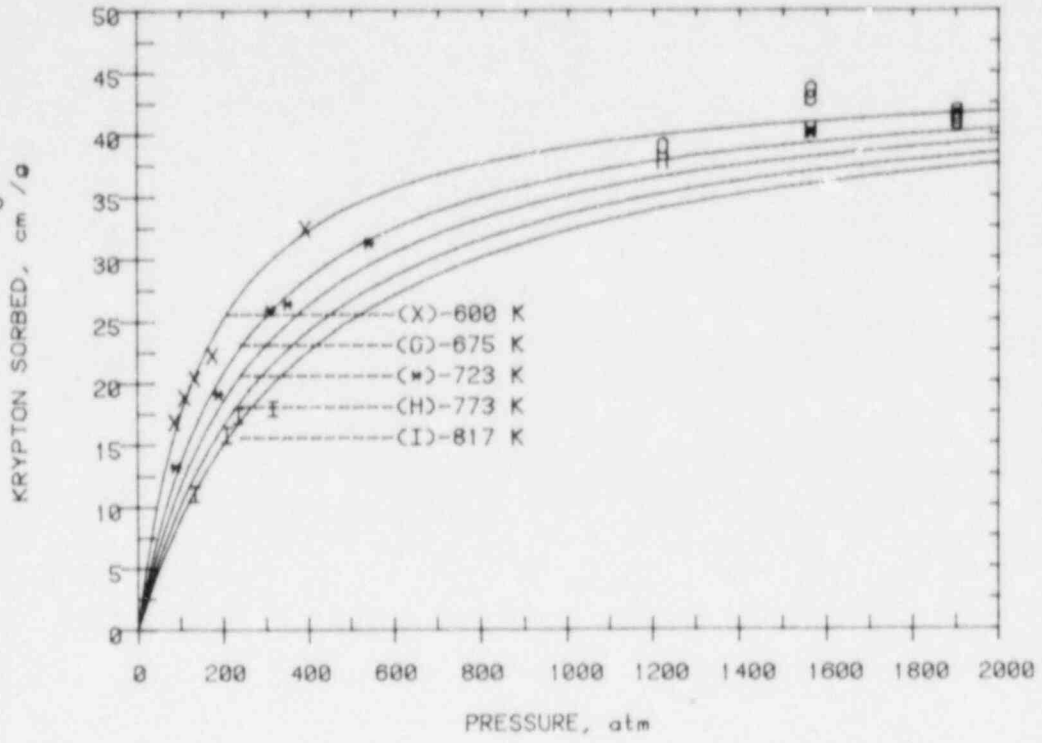


Figure II-8. Isotherms for equilibrium krypton loadings on leached sodalite fit to experimental data using the Langmuir model.

These combined results were used to generate theoretical equilibrium isochores (lines of constant loading) for krypton in sodalite as a function of pressure and temperature, as shown in Figure II-9. The isochores can be used to estimate maximum loading that might be achieved at temperatures and pressures outside the range of the experimental apparatus.

When mixtures of krypton and xenon were used, very little xenon was encapsulated. Equilibrium krypton loadings are shown in Figure II-10 for different krypton-xenon mixture compositions. The amount of krypton encapsulated gradually decreases as the xenon composition of the gas increases, as predicted from Henry's law. The decrease in krypton loading was only 25 to 30% when a little less than twice as much xenon than krypton is present in the gas phase. The xenon loading under the high xenon composition was only about 1 and

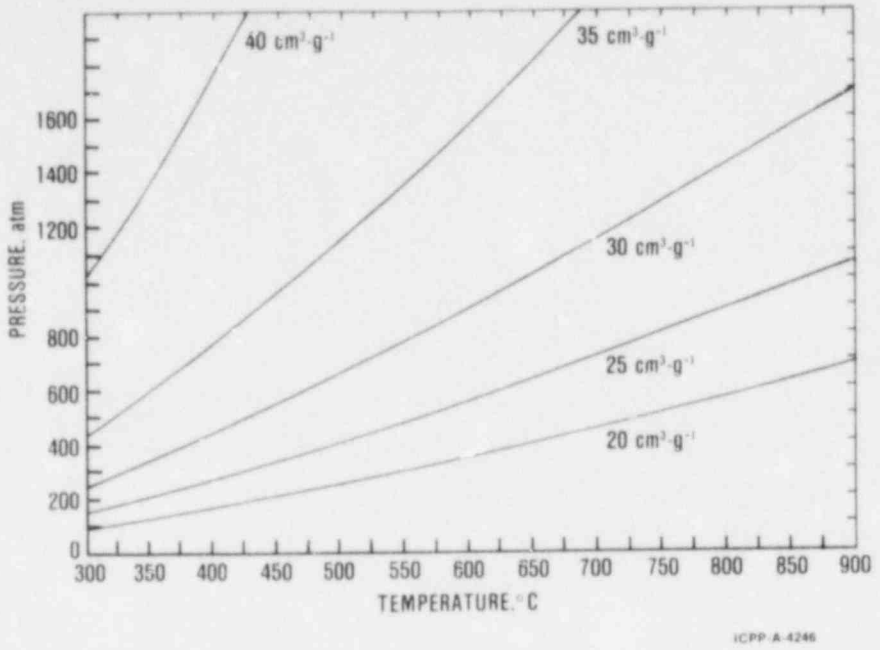


Figure II-9. Isochores for equilibrium krypton loadings on leached sodalite using the Langmuir model fit of experimental data.

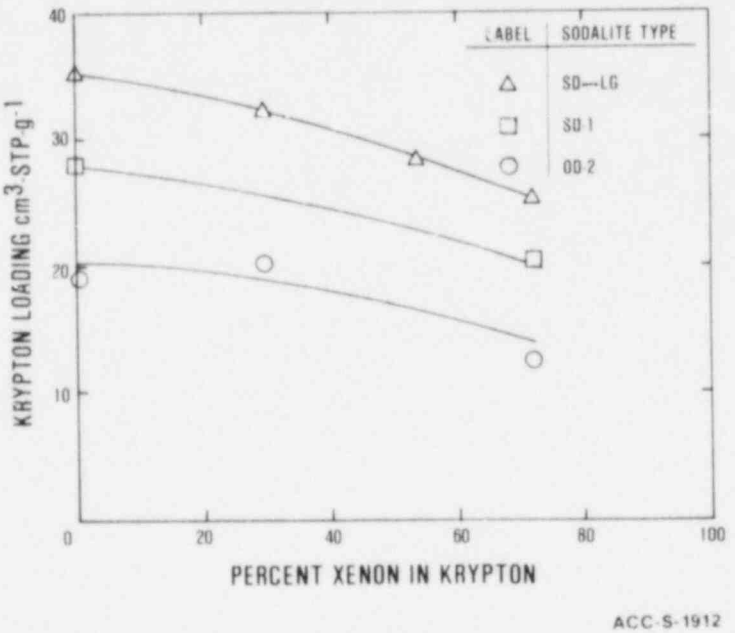


Figure II-10. Equilibrium krypton loading in sodalites as a function of gas composition at 500°C and 1220 atm.

5 $cm^3$STP $g^{-1}$ for oven-dried and spray-dried sodalites, respectively. Apparently the difference in krypton and xenon molecular diameters is great enough to almost completely exclude xenon from sodalite.

## 3.2 Rates of Encapsulation

3.2.1 Screening Tests. Zeolite, glasses, aluminum, carbons, and other sorbents were tested for their potential application to krypton immobilization. Krypton loadings are shown in Table II-I for the materials. On those materials for which promising loadings were measured, further leakage tests were made to determine their storage feasibility. Of all the materials shown in Table II-I, only sodalite was found to have satisfactory loading and leakage characteristics (see Section II-3.3 for leakage results).

TABLE II-I

RESULTS SCREENING TESTS FOR KRYPTON ENCAPSULATION IN VARIOUS MATERIALS

| Name | Temperature, °C | Pressure, atm | Time, h | Kr Loading, $cm^3$ STP/g | Xe Loading, $cm^3$ STP/g |
|---|---|---|---|---|---|
| Unleached oven-dried sodalite | 500 | 1910 | 24 | 25 | -- |
| Leached oven-dried sodalite | 500 | 1910 | 24 | 41 | -- |
| K-exchanged A[a] pills | 500 | 1910 | 24 | 73 | -- |
| Rb-exchanged on Na A[a] pills | 500 | 1910 | 24 | 56 | -- |
| Cs-exchanged on Na A[a] pills | 500 | 1910 | 24 | 61 | -- |
| Rb-exchanged on K A[a] pills | 500 | 1910 | 24 | 36 | -- |
| K-exchanged erionite powder | 500 | 1910 | 24 | 16 | -- |
| K-exchanged erionite granules | 500 | 1910 | 24 | 22 | -- |
| K-exchanged chabazite granules | 500 | 1910 | 24 | 7 | -- |
| Synthetic Na chabazite powder | 400 | 1520 | 3 | >1 | -- |

TABLE II-I (continued)

| Name | Temperature, °C | Pressure, atm | Time, h | Kr Loading, $cm^3$ STP/g | Xe Loading, $cm^3$ STP/g |
|---|---|---|---|---|---|
| Vycor thirsty glass | 500 | 1910 | 24 | 6 | -- |
| Quartz fiber | 500 | 1910 | 24 | 6 | -- |
| Silica gel #62 | 500 | 1910 | 24 | 3 | -- |
| Aluminum 201 | 500 | 1910 | 24 | 3 | -- |
| Reticulated vitreous carbon, crushed | 500 | 1910 | 24 | 1 to 80 | -- |
| Exfoliated graphite | 500 | 1910 | 24 | 6 | -- |
| Coconut charcoal | 500 | 1910 | 24 | 3 | -- |
| Ambersorb | 500 | 1910 | 24 | 0.9 | -- |
| Nosean | 500 | 1220 | 72 | 0.4 | 0.04 |
| Chlorosodalite | 500 | 1220 | 1.5 | .06 | .007 |
| Cs-exchanged erionite | 500 | 1220 | 0.5 | 0.2 | 0.4 |
| Rb-exchanged erionite | 500 | 1220 | 72 | 0.4 | 4 |

a. A refers to Zeolite A.

Initial testing with sodalite used argon instead of krypton. Table II-II compares typical Ar and Kr loadings. In general, the argon was encapsulated more rapidly than krypton at any given temperature.

TABLE II-II

LOADINGS OF ARGON AND KRYPTON ON SODALITE AT 360°C and 4 h

| Gas | P, atm | Leached Sodalite | Unleached Sodalite |
|---|---|---|---|
| Ar | 1910 | 21 | 38 |
| Ar | 710 | -- | 32 |
| Kr | 1910 | 11 | 1 |

3.2.2 Krypton Encapsulation Tests. Krypton encapsulation results using spray-dried sodalite and oven-dried sodalite are shown in Figures II-11 and II-12, respectively. All curves show an initially rapid loading with a gradual slowing down as the equilibrium loading is approached. The temperature had a strong effect on encapsulation rates, as would be expected with an activated diffusion mechanism. Leached sodalites (SD-1-L48H and OD-2-L48H) in which most of the intercalated sodium hydroxide had been removed were encapsulated much more rapidly than were unleached samples (SD-1, OD-2). The leaching beyond 12 h did not increase the krypton loading significantly. Leached oven-dried and spray-dried samples behaved similarly, while unleached spray-dried samples were encapsulated more rapidly than were unleached oven-dried samples. Pilling had an effect on krypton loading only when a significant (~10 wt%) amount of binder was present as an inert diluent, with a corresponding (about 10%) decrease in loading per unit weight.

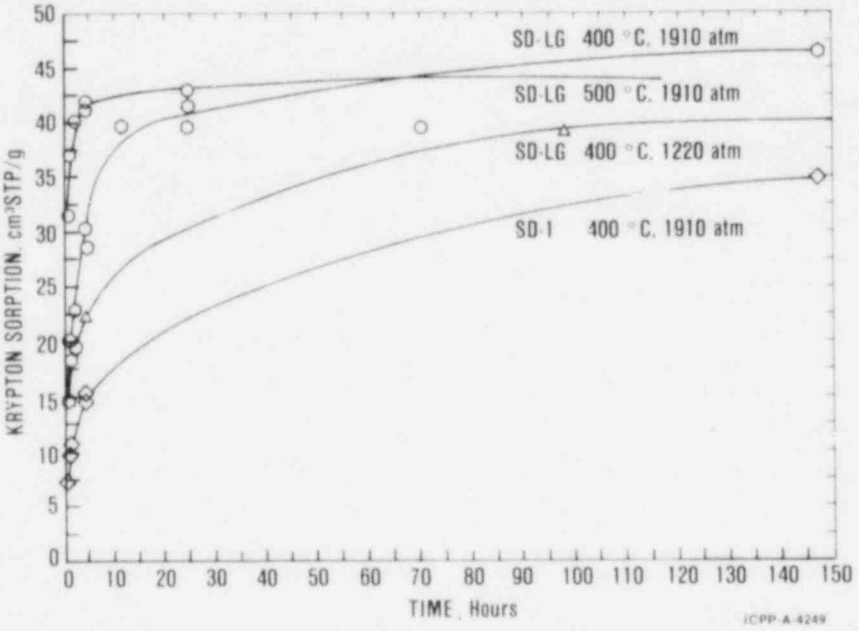


Figure II-11. Krypton loading on spray-dried sodalite as a function of time at various temperatures, and pressure of pure krypton.

One experiment was used to check leached sodalite powder for different loadings at different sample positions in a large sample volume. The sodalite sample was placed in each of two cylindrical containers:

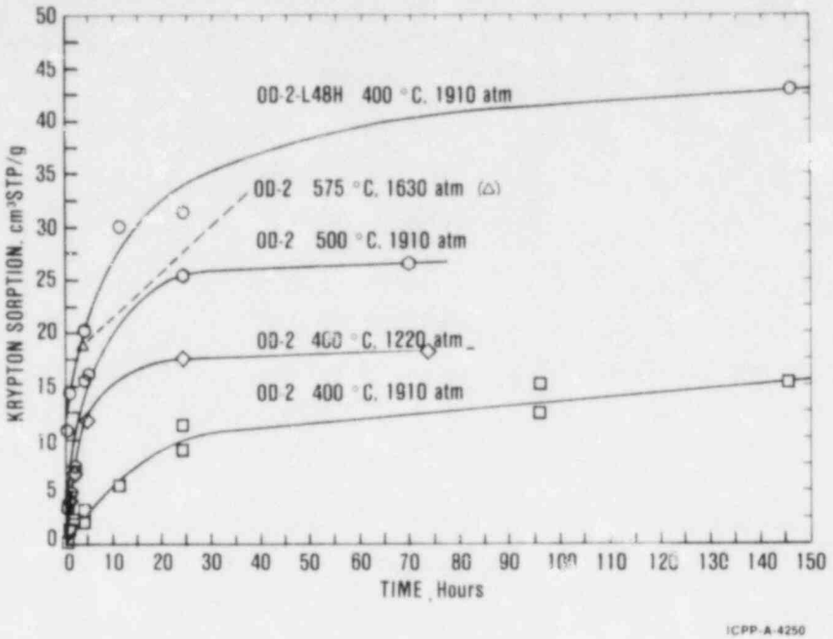


Figure II-12. Krypton loading on oven-dried sodalite as a function of time at various temperatures, and pressure of pure krypton.

(1) 0.75 cm-diameter x 8 cm long, containing 4 g

(2) 3 cm-diameter x 10 cm long, containing 80 g

Both samples sorbed 39 $cm^3/g$ and no difference was observed in the top, center, and bottom of container (2).

The previous results showed that equilibrium loadings (~30 to 40 $cm^3/g$) were reached in leached oven- and spray-dried sodalites in a few hours at 500°C. Since longer times were required with unleached sodalite to load ~20 to 25 $cm^3/g$ of krypton at 500°C, experiments at 575°C and 2 and 4 h were made. A pressure of 1630 atm was used to allow for a large safety margin on the vessel stress.

The following loadings were achieved:

| Unleached Sodalite Type | Loading, $cm^3/g$ |
|---|---|
| OD-2 Powder | 22 at 2h |
| SD-1 Pills | 24 at 2h |
| SD-2, K-exchanged | 26 at 4h |
| SD-LG | 40 at 2h |

Previous OD-2 loadings at 500°C and 4 h were ~15 $cm^3/g$ at 1910 atm and ~12 $cm^3/g$ at 1220 atm. Thus the higher loading at 575° and 1630 atm looks very promising. The pilled SD-1 and powdered OD-2 both have very low leakage rates, as reported in the next section. Leakage measurements for potassium-exchanged sodalite have not yet been made, but should be lower than for unexchanged sodalite. Thus the higher loadings at 575°C show that a commercial-scale encapsulation system could be operated at one run per day and that the encapsulation process is feasible for OD-2 powder, K-exchanged OD-2 powder, and SD-1 pills.

Figure II-13 shows the rates of encapsulating krypton from various krypton-xenon mixtures using spray-dried and oven-dried sodalites. A comparison with theoretical pure Kr loading is given in Section 3.2.3.

3.2.3 Model of Rate of Encapsulation. Equation (12) was modeled to fit experimental data by allowing D to be the fitting parameter. The calculated rates of encapulation are compared with experimental data at 1910 atm and different temperatures in Figure II-14 for

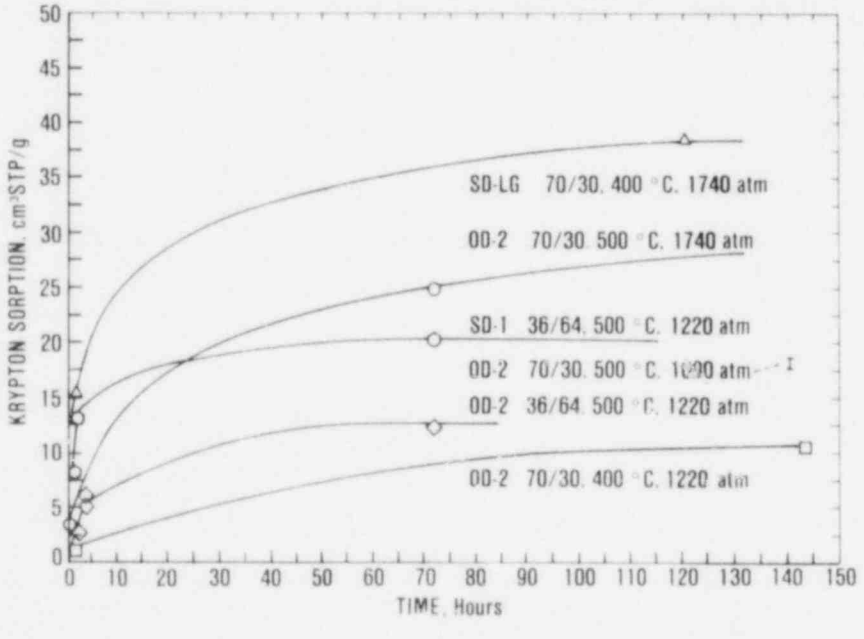


Figure II-13. Krypton loading on sodalites as a function of time at various temperatures, pressures, and krypton-xenon gas compositions given as Kr/Xe ratios, e.g, 70/30.

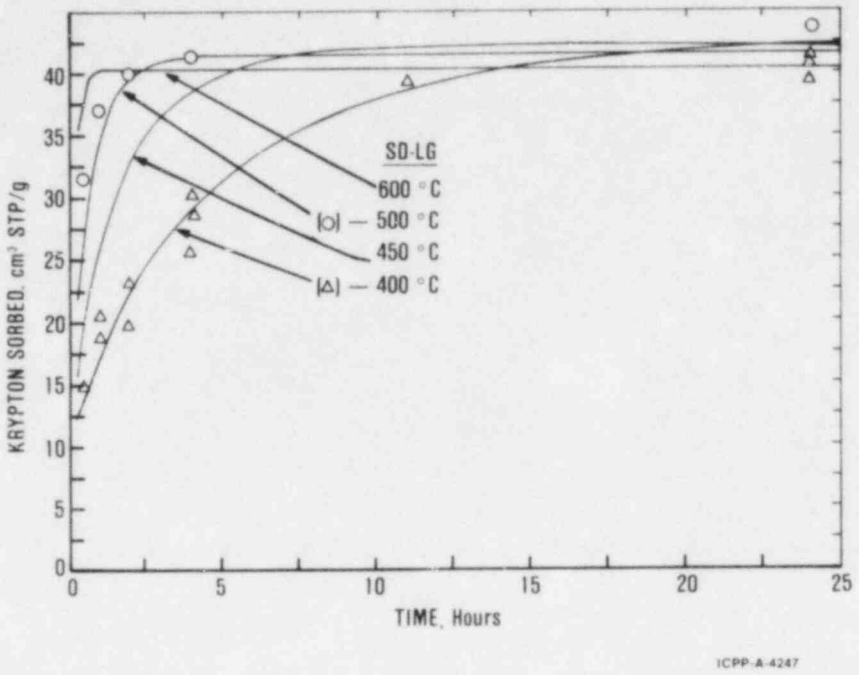


Figure II-14. Comparison of calculated rates of krypton loading on leached sodalite, SD-LG, at 1910 atm and various temperatures with experimental data at 400 and 500°C.

leached sodalite and in Figure II-15 for unleached sodalite. Since equilibrium sorption data for OD-2 was not obtained at the INEL, the equilibrium sorption data measured by Vaughan for unleached sodalite was used. The values of D which were used to fit the loading rates are compared with D calculated from leakage rates in Section 3.3.1 (see Figure II-20).

The calculated rates of loading on unleached sodalite (OD-2) with pure krypton are compared with measured rates in krypton-xenon mixtures in Figure II-16. Since mixing effects are not known, loading curves for each sodalite type were calculated assuming a krypton pressure equal to the total krypton-xenon mixture pressure and assuming a krypton pressure equal to the partial pressure of krypton in the krypton-xenon mixture. In either case, the rate of krypton encapsulation is not much lower in the krypton-xenon mixture than it is in pure krypton. Any further conclusions can be drawn only after the theory is modified for gaseous mixtures and more experimental data is available.

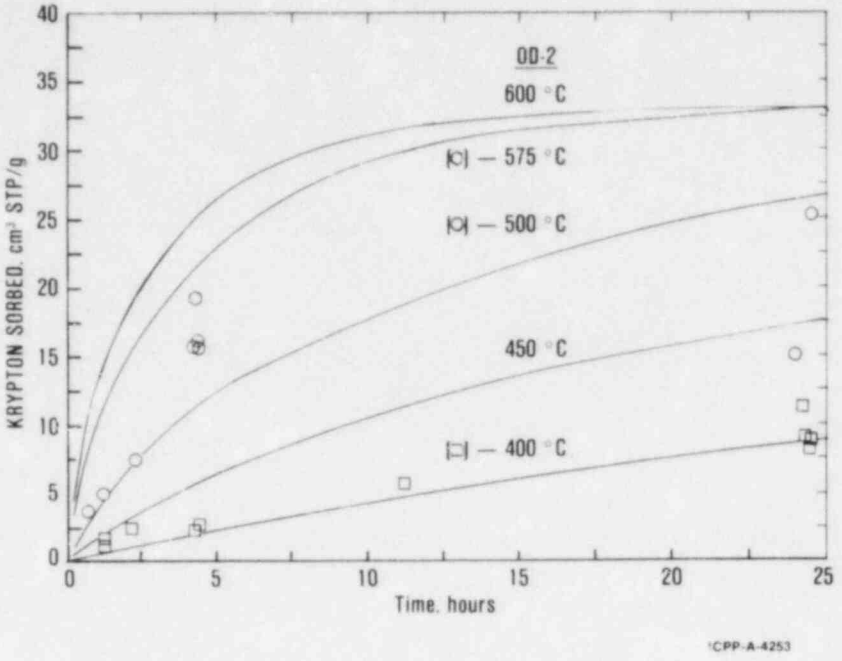


Figure II-15. Comparison of calculated rates of krypton loading on unleached sodalite, OD-2, at 1910 atm and various temperatures with experimental data at 400, 500, and 575°C.

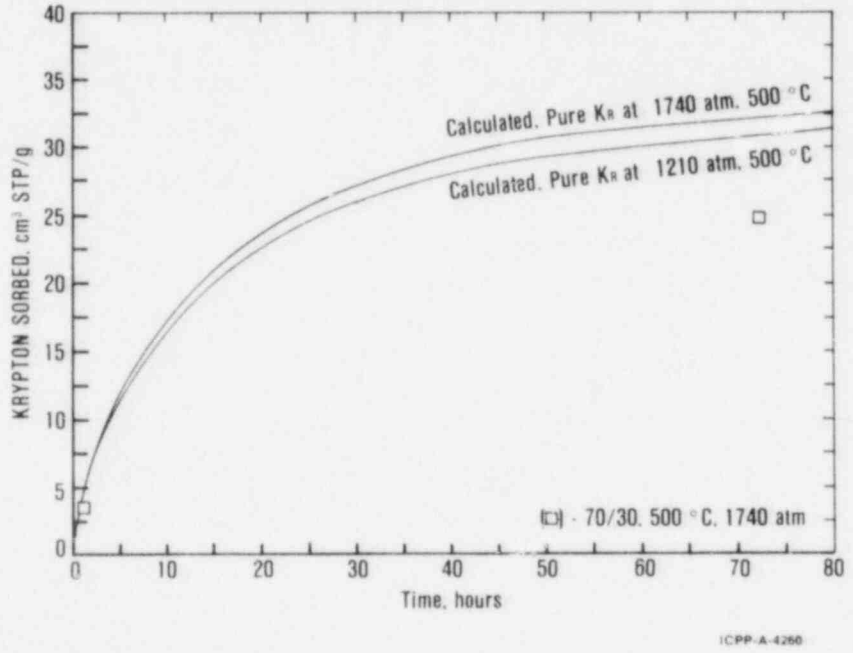


Figure II-16. Comparison of experimental Kr loadings from Kr-Xe mixtures with calculated Kr loadings from pure krypton at 500°C using unleached sodalite OD-2.

## 3.3 Krypton Leakage Measurement

3.3.1 High Temperature Tests (300 to 500°C). Typical rates of leakage of krypton from unleached sodalite OD-2 at several temperatures are shown in Figure II-17. The calculated diffusivities show an Arrhenius behavior in Figure II-18 for leached and unleached samples of spray-dried and oven-dried sodalites. Within experimental error (~±5 kcal/ mole) the activation energy (or slope) is not markedly different for leached and unleached materials, but it is different for spray-dried and oven-dried materials. Vaughan did find different activation energies for his leached and unleached samples.[41,44] Vaughan's leached and unleached data are compared with SD-LG and OD-2 in Figure II-19.

The effect of initial krypton loading on diffusivity can be seen in Figure II-20. The decreased loading results in a lower activation energy. If this effect can be extrapolated to storage temperatures (about 150°C), samples with low loading would not be good for long-term storage.

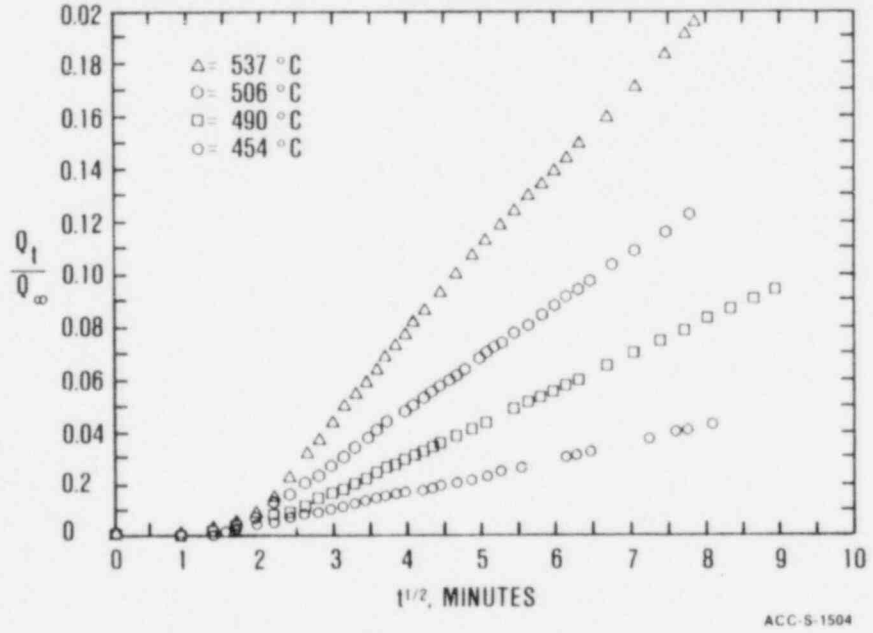


Figure II-17. Typical rates of fractional leakage of krypton encapsulated in unleached sodalite at various temperatures.

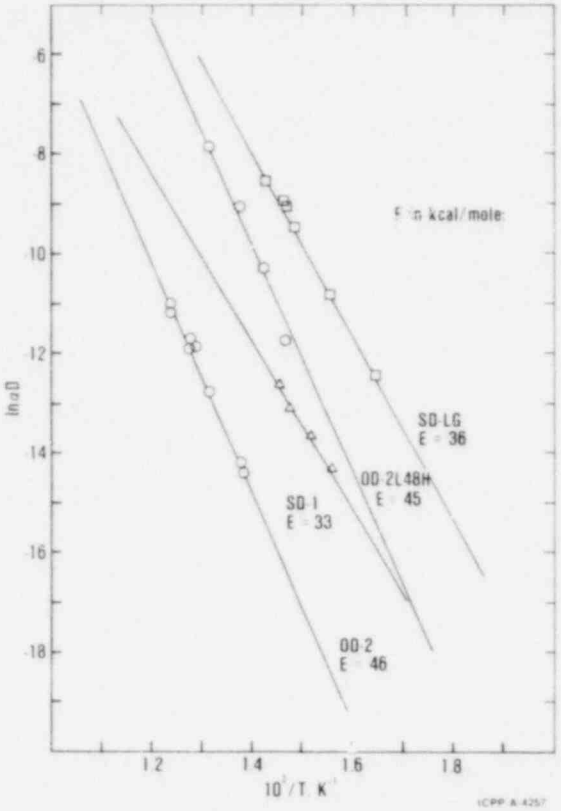


Figure II-18. Temperature dependence of diffusion of krypton in leached and unleached sodalites SD and OD. See Equation (13) for $\alpha$.

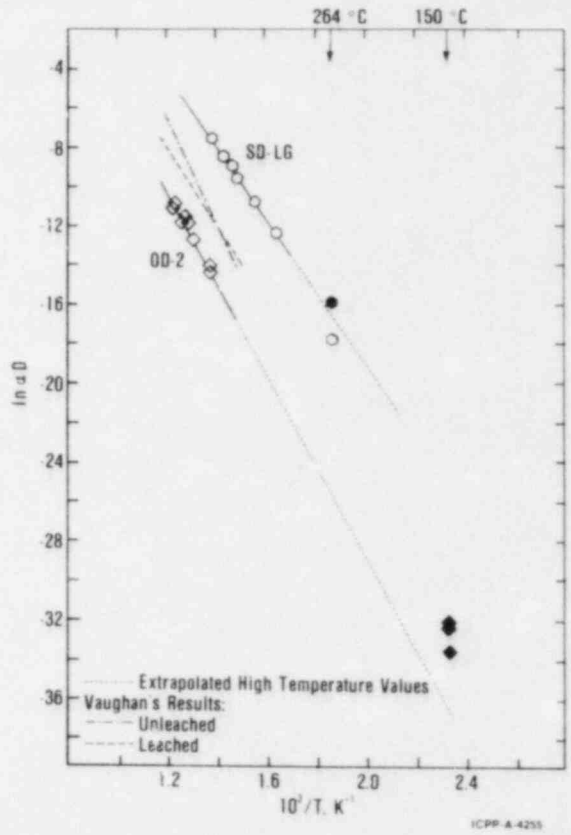


Figure II-19. Comparison of the temperature dependence of diffusion of krypton in OD-2 and SD-LG with Vaughan's results and with 264 and 150°C leakage measurements. High-temperature method used for open points; low-temperature method for filled points.

Diffusivities measured in sodalite pills are not significantly different from those measured in powder. The macropore (intercrystalline) diffusion is evidently much more rapid than micropore (intracrystalline) diffusion.

The effects of adsorbed water and co-adsorbed xenon on spray-dried sodalite samples are shown in Figure II-21. Leakage runs were made with two samples initially containing high adsorbed water after they were treated to remove some of the water. The samples were evacuated; one at 150°C for ∿16 h, the other at 25°C for ∿500 h. In both cases, the leakage rate (or diffusivity) in Figure II-21 was slightly slower than the corresponding untreated samples.

A series of runs was made with SD-LG encapsulated with a 50/50 Kr/Xe mixture, resulting in Kr and Xe loadings of 29 and 2 cc/g, respectively. After encapsulation, samples were kept in a dry glove box before leakage measurements were made. The krypton diffusion coefficients were significantly lower for the Kr/Xe mixture at low adsorbed water vapor conditions.

While it is not possible to determine the relative contribution of each effect, krypton leakage rates at high temperatures are reduced when little water vapor is adsorbed and when xenon is present during encapsulation.

3.3.2 Long-Term Storage Tests (50 to 300°C). Screening tests were run at 150°C for one month and all materials except sodalite lost from 50 to about 100% of the krypton (see Table II-III). Leached sodalite leaked more rapidly than unleached. Sodalite with high adsorbed water content leaked krypton much more rapidly than did sodalite with low adsorbed water. Sodalite with added xenon leaked less rapidly than without Xe. Oven-dried sodalite with low adsorbed water content leaked the least. Because of these results, only sodalite was considered for further long-term storage tests.

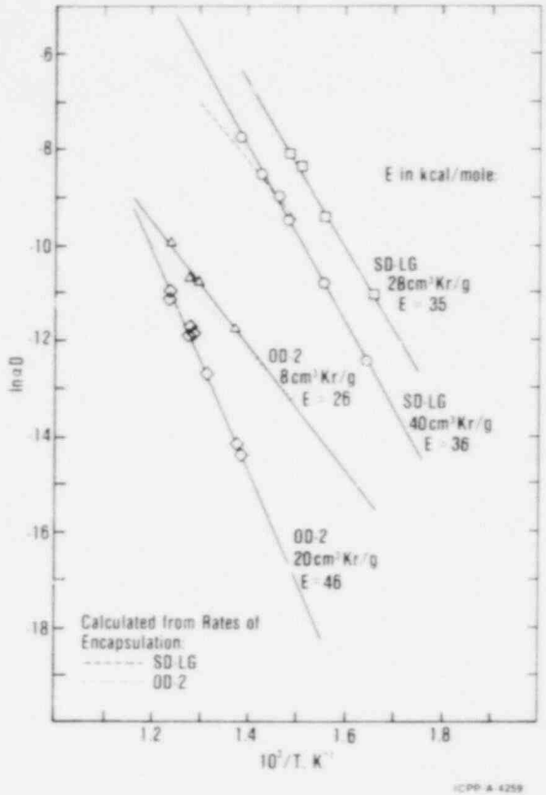


Figure II-20. Effect of initial concentration of encapsulated krypton on the temperature dependence of diffusion of krypton in sodalite. See Equation (13) for α.

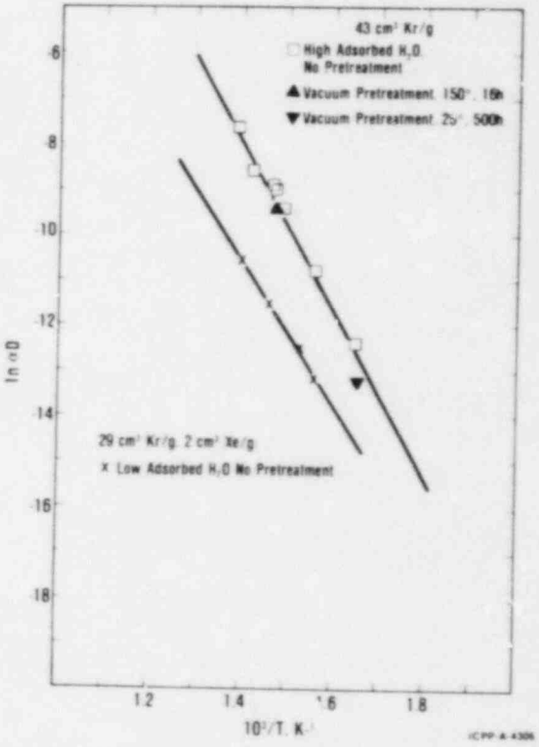


Figure II-21. Effects of absorbed xenon and water on the temperature dependence of diffusion of krypton in leached sodalites.

TABLE II-III

RESULTS OF SCREENING TESTS FOR KRYPTON LEAKAGE IN ONE MONTH AT 150°C

| Material | Adsorbed $H_2O$ Gaseous $cm^3/g$ | Initial Kr Loading, $cm^3/g$ | % Leakage |
|---|---|---|---|
| K-Exchanged Zeolite A | 141 | 73 | 100 |
| Rb-Exchanged Zeolite A | 116 | 56 | 99 |
| Cs-Exchanged Zeolite A | 75 | 61 | 97 |
| K-Exchanged Erionite | 64 | 16 | 57 |
| Vitreous Carbon | -- | 80 | 54 |
| Sodalite[a], SD-LG | 62 | 38 | 9 |
| Sodalite[a], SD-LG, Added Xe[b] | 56 | 35 | 6 |
| Sodalite[a], SD-LG | 6 | 43 | 0.7 |
| Sodalite[a], SD-1 | 5 | 35 | 0.6 |
| Sodalite[a], OD-2 | 10 | 21 | 0.1 |

a. SD is spray-dried; OD is oven-dried; L means leached.

b. Xe = 3 $cm^3/g$ was sorbed from Kr/Xe = 0.7 mixture.

Although sodalite had been thoroughly dried before encapsulation, some samples were allowed to sorb varying amounts of water vapor from ambient to see if the water helped to block krypton release at 150°C. Figure II-22 shows long-term leakage measurements at 150°C with samples containing different amounts of krypton and adsorbed water. For samples with similar water content, but with approximately a two-fold difference in krypton loading, the sample with a lower krypton concentration leaked much more rapidly. When the water content is greater than approximately 10 gaseous $cm^3/g$, krypton leaks more rapidly. However, if it is less than 10 $cm^3/g$, krypton also leaks more rapidly. Thus, water may block the cage openings a low concentration, but assist with krypton leakage at higher concentrations.

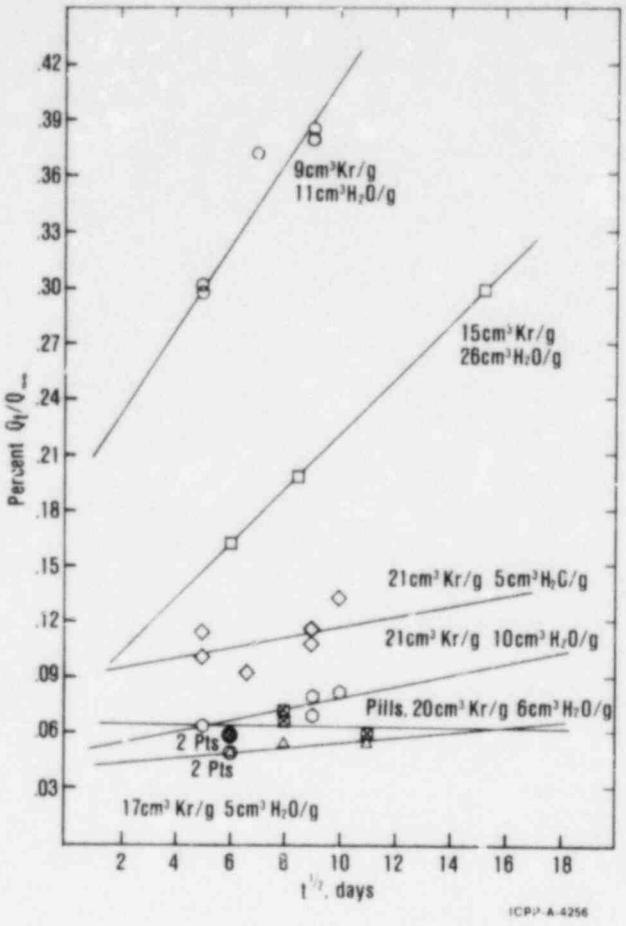


Figure II-22. Rates of percent leakage at 150°C of krypton encapsulated in unleached sodalite at various Kr loadings and amounts of adsorbed water.

For OD-2, the amounts of absorbed water were always less than for SD-LG, where up to 60 gaseous $cm^3/g$ had been observed. This may be due to over-leaching of sodium in SD-LG. The OD-2 sample containing 20 $cm^3/g$ Kr and 10 $cm^3/g$ $H_2O$ was obtained by allowing the material with 5 $cm^3/g$ $H_2O$ to sit for 14 h in air saturated with water vapor at 25°C, a much more severe condition than normal atmospheric water vapor concentration.

Although some of the leakage rates appear high as plotted in Figure II-22, the extrapolation to ten years for the worst case is about 1.6% leakage of total Kr. The other five samples would leak from ~0.05% to about 1% in ten years. Table II-IV gives the percent and the 95% confidence limit of krypton leakage from sodalite at

150°C and 10 years, as calculated from the lines in Figure II-22. The percent leakage of $^{85}Kr$ is nearly half of the values shown in Table II-IV at ten years due to radioactive decay. After ten years, the exponential rate of radioactive decay becomes more important than the square-root rate of leakage, and the total inventory of krypton-85 outside of the sodalite, but inside a cannister, decreases (see Figure II-5). Thus any of these results would predict low krypton release at a long-term storage temperature of 150°C.

Unleached spray-dried sodalite samples that had been pilled were found to have identical leakage rates when compared with unleached oven-dried powdered samples, for similar krypton loadings and adsorbed water content. The apparent negative slope in Figure II-22 for the pilled material is probably due to the fact that the leakage rate was so low that it was obscured by experimental error.

TABLE II-IV

PREDICTED PERCENT LEAKAGE AT 150°C AND 10 YEARS FOR ENCAPSULATED KRYPTON FROM UNLEACHED SODALITES

| Sample Type[a] | Initial Loading, Gaseous $cm^3/g$ | | Predicted Percent Leakage at 150°C and 10 Years[b] |
|---|---|---|---|
| | Kr | $H_2O$ | |
| OD-2 | 9 | 11 | 1.6 ± 1.1 |
| OD-2 | 15 | 26 | 1.0 ± 0.1 |
| OD-2 | 21 | 5 | 0.3 ± 0.5 |
| OD-2 | 21 | 10 | 0.2 ± 0.4 |
| SD-1, Pills | 20 | 6 | 0.05 ± 0.3 |
| OD-2 | 17 | 5 | 0.1 ± 0.2 |

a. Powdered, unless otherwise specified.

b. 95% confidence interval included.

In samples with added xenon, much larger fractions of xenon are released initially, indicating that much of the xenon is not trapped far from the crystal surface. In general, the added xenon did slow the krypton leakage rates for samples with similar krypton loading and adsorbed water content.

3.3.3 Comparison of High Temperature and Long-Term Storage Tests. An intermediate temperature, 264°C, was chosen for leakage measurements using each of the high- and low-temperature methods (see Section II-2.2 for a description of the methods). Using the long-term storage (low-temperature) method, four sets of duplicate samples were placed in a 264°C oven and removed at 1, 4, 10.5, and 22.5 h for mass spectrometric analysis. Due to variation in adsorbed water on these samples, there was some scatter in the duplicate analyses. The high-temperature method was run for 40 h, with periodic analysis of leaked krypton using the gas chromatograph. The calculated diffusivities are shown in Figure II-19. Within the range of experimental error, the low-temperature and high-temperature results fit on the extrapolated Arrhenius plot. Further experiments in this temperature region are required to show any differences other than experimental error.

Leakage rates from long-term storage tests at 150°C in Figure II-22 are mostly higher than the value extrapolated from high temperature measurements in Figure II-19. In the case of pilled sodalite, the rate in Figure II-22 (or diffusivity) appears negative and is not included on Figure II-19. There is evidence that these higher values in Figure II-19 are due to a rapid initial leakage rate which may be followed by a slower component. Other data of leached sodalite at 150°C and at higher temperatures show more pronounced evidence of such behavior. The initial leakage appears to be a few tenths' of percent for sample with low adsorbed water and a few percent for samples with high adsorbed water. Further measurements are required to verify this behavior.

3.3.4 Gamma Radiation Tests. Samples of sodalite containing encapsulated krypton were placed in quartz tubes, evacuated, and sealed. The tubes were positioned in a high gamma radiation field at the INEL for 105 days, resulting in a total exposure of $2 \times 10^9$ rads. The temperature varied between 48 and 115°C, with a daily average of 60°C. The radiation field had no detectable effect on krypton release rates when compared with laboratory control samples. However, a small amount of hydrogen but almost no oxygen was formed. Previous work at Savannah River Laboratories reports similar behavior of $H_2$ formation with almost no $O_2$ formation.[60]

## 3.4 Technical Feasibility Evaluation

Krypton loadings on sodalite of 20 to 40 $cm^3/g$ would provide a storage medium volume which is similar to krypton in a pressurized cylinder at 16 to 32 atm, respectively. Unleached sodalite has been encapsulated up to about 20 $cm^3.g$ in 2 h at 575°C and 1630 atm. This rate would allow a commercial process to operate at the rate of one batch per day, using one high pressure vessel.

Equilibrium krypton loadings at 500°C in sodalite are not lowered greatly (less than 15%) when large quantities of xenon are present (Kr/Xe = 0.5) and very little (~1 $cm^3/g$) Xe is loaded. Thus krypton will not have to be purified of excess xenon to very high levels to provide feasible equilibrium loadings. Kinetic data is not yet available for krypton-xenon mixtures at 575°C or higher to determine what purity requirements might be needed to allow a commercial process to operate at one batch per day. From results at 500°C, a Kr/Xe = 0.7 mixture should also be feasible.

Krypton leakage rates from unleached sodalite measured at a storage temperature of 150°C for one year were typically less than that which would give 1%, and as little as 0.05% leakage in ten year's storage. While the amount of initial krypton loading and adsorbed water showed some effect on the predicted ten-year leakage rate, most samples were within the 1% leakage in ten years. The amount of water

which might be sorbed at typical long-term storage conditions needs to be determined. When the sodalite was loaded with small amounts of xenon, the resulting krypton leakage rate was lowered.

There is some evidence from the long-term leakage studies at 150°C that there are two distinct leakage rates over a one-year span: a more rapid rate followed by a slower rate. Such behavior could arise from initial rapid diffusion of surface-adsorbed krypton in damaged portions of the crystal, followed by diffusion of trapped krypton through the sodalite cage network. Further work is required to verify such behavior.

While unleached sodalite appears to be a technically feasible material to encapsulate krypton-85, based on this report, the use of partially leached sodalites should not be ruled out. Most of the leached sodalite samples which were used had been leached at too stringent conditions. In addition to removing most of the intercalated NaOH, some of the structural sodium cation was exchanged with hydrogen, resulting in a more accessible pore structure and in leakag rates somewhat higher than in unleached sodalite. A sodalite with an optimum sodium hydroxide content has probably not yet been developed and needs further experimentation.

All of the leakage studies were carried out in vacuum. Further studies should be made in which the sodalite sample is contained in a cover gas such as dry or humid air or an inert gas, to simulate storage conditions more closely.

Preliminary studies show that sodalite is not damaged or encapsulated or krypton is not released in a high gamma radiation field ( $2 \times 10^9$ rads). The formation of small quantities of hydrogen during irradiation needs to be studied further to determine possible limits for long-term storage. As the decay product, Rb, is formed, it will probably remain in its cage and help block Kr leakage.[70] Long-term leakage studies need to be made with sodalite containing krypton-85.

# III. ECONOMIC FEASIBILITY

An evaluation of the economic feasibility can be made based on the process shown to be technically feasible in Section II, i.e., krypton encapsulation in unleached oven-dried sodalite OD-2. A preliminary design and cost estimate of the commercial-scale plant that can encapsulate the maximum amount of krypton released in the dissolver off-gas of a reference fuel reprocessing plant will be given. The reference reprocessing plant used is that presented in the DOE document, Draft Environment Impact Statement. Management of Commercially Generated Radioactive Waste.[15] An evaluation of the availability of the necessary technology and of major unresolved problems will be made.

## 1. Preliminary Design and Cost Estimate of a Commercial-Scale Encapsulation Facility

### 1.1 Design Basis

Table III-I gives the basis used in preparing the preliminary design and cost estimate. The krypton-85 released in the dissolver off-gas was assumed to be recovered at a 100% recovery efficiency, not at the 90% efficiency assumed in Reference 15, in order to provide a conservative estimate of plant scale.

### 1.2 Preliminary Design

Figure III-1 shows the preliminary floor plan design for a krypton-85 encapsulation facility. The building consists of two floors, one totally below ground and one at ground level. The encapsulation process is located in the basement level, with access parts directly above parts of the process area, on the ground level. A control room, cold storage area, office, and laboratory take up the rest of the facility.

TABLE III-I

BASIS FOR COMMERCIAL-SCALE ZEOLITE ENCAPSULTATION FACILITY DESIGN AND COST ESTIMATE

| | Case I | Case II |
|---|---|---|
| Total operating time, days/year | 300 | 300 |
| Annual capacity[a], MCi | 18.7 | 18.7 |
| Gas composition[b], $\%^{85}Kr$ | 5.4 | 3 |
| % Total krypton | 90 | 50 |
| % Xe | 10 | 50 |
| Process feed lag storage[c], MCi | 3.7 | 3.7 |
| , No. of cylinders[d] | 12 | 18 |
| Interim encapsulated product storage[e]-MCi | 1.9 | 1.9 |
| -No[d] canisters | 30 | 30 |

a. Assuming annual $^{85}Kr$ recovery from dissolver off-gas of 17 MCi and 110% capacity.

b. Assuming $^{85}Kr$ as 6% of total krypton.

c. Assuming capacity for krypton-85 recovered in 60 days at 110% capacity.

d. Assuming 49.6 L, DOT-3AA-2400 cylinders with total pressure of 2000 psi per cylinder.

e. Assuming storage capacity for 30 days' production, one canister per day, and 110% capacity.

Figure III-2 is a schematic of an encapsulation system required for radioactive service. The layout of the various components is shown in Figure III-1, Basement Level.

1.2.1 Process Description. A porous metal capsule filled with zeolite pellets is inserted into the pressure vessel using a manipulator and/or overhead crane. The vessel is remotely closed, sealed, and evacuated at the encapsulation temperature using the mechanical vacuum pump in Figure III-1 (or V2 in III-2). After activation is

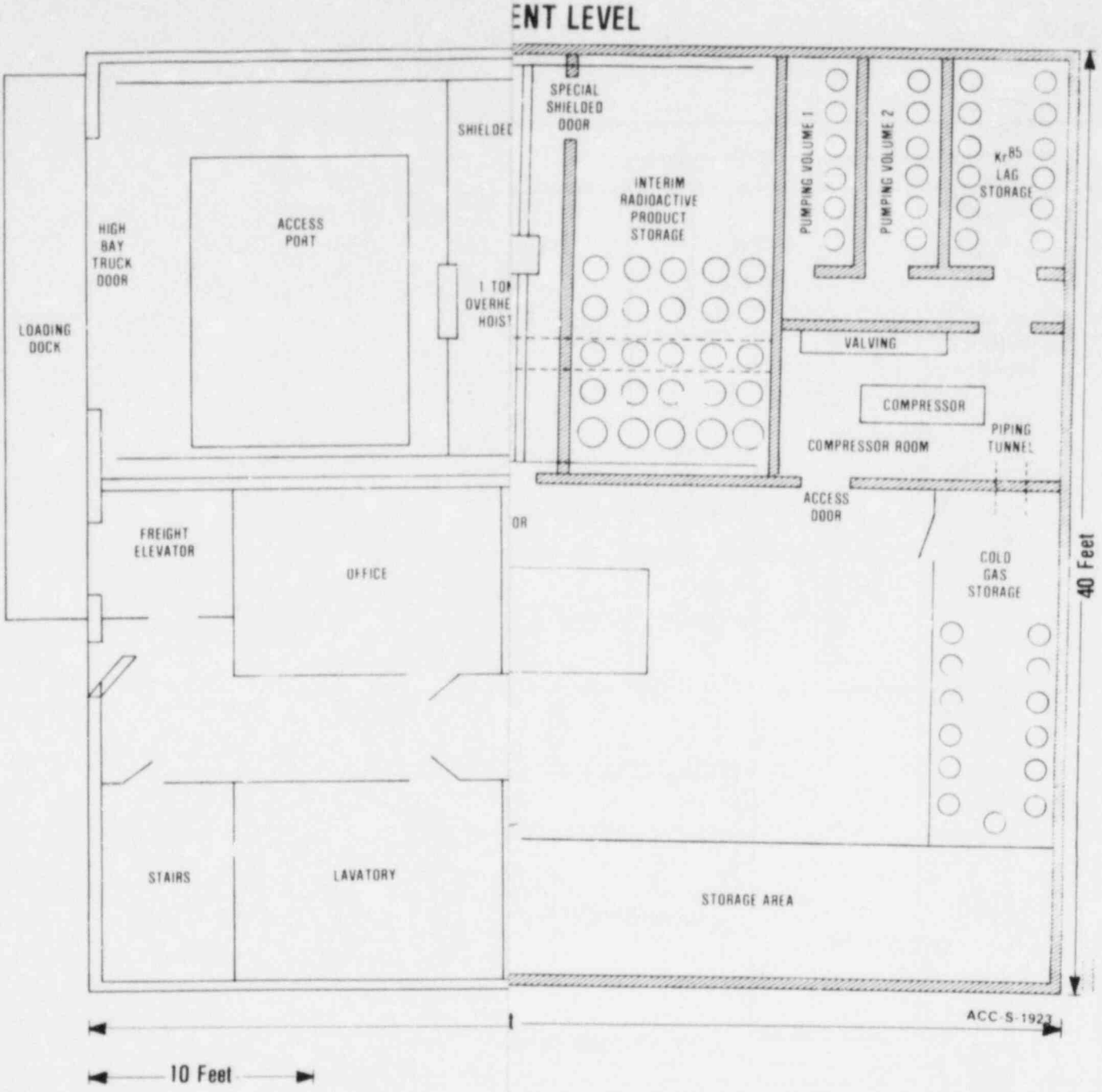
ENT LEVEL
SPECIAL SHIELDED DOOR
SHIELDED
PUMPING VOLUME 1
PUMPING VOLUME 2
$Kr^{85}$ LAG STORAGE
INTERIM RADIOACTIVE PRODUCT STORAGE
ACCESS PORT
HIGH BAY TRUCK DOOR
LOADING DOCK
VALVING
COMPRESSOR
COMPRESSOR ROOM
PIPING TUNNEL
ACCESS DOOR
FREIGHT ELEVATOR
OFFICE
COLD GAS STORAGE
40 Feet
STAIRS
LAVATORY
STORAGE AREA
ACC-S-1923
10 Feet

PRESSURE COMPRESSOR ASSEMBLY

PRESSOR
Y

2-30 KPSI COMPRESSOR ASSEMBLY

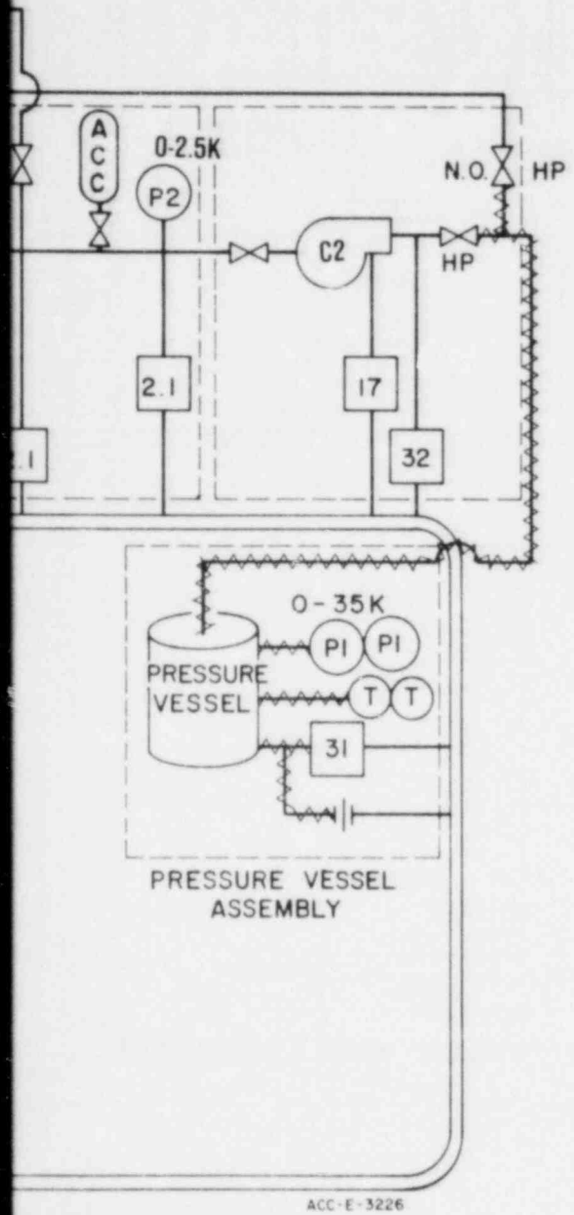


**LEGEND**

- COMPRESSOR
- R — PRESSURE REGULATOR
- 21 / 0-3K — PRESSURE RELIEF VALVE, 21 KPSI
- P — PRESSURE GAUGE 0-3000 PSI RANGE
- Pv — VACUUM PRESS. GA., atm - 1m TORR
- A — VENT TO ATMOSPHERE
- T — TEMPERATURE GAUGE - DIGITAL READOUT
- V — VACUUM PUMP
- B — BELLOWS VALVE, NORMALLY CLOSED
- ACC — ACCUMULATOR
- N.O. — NORMALLY OPEN VALVE, MEDIUM PRESSURE
- NORMALLY CLOSED VALVE MEDIUM PRESSURE
- LOW PRESSURE TUBING
- MEDIUM PRESSURE TUBING
- HIGH PRESSURE TUBING
- RELIEF VALVE DISCHARGE TUBING
- RUPTURE DISC., SET PER ASME CODE
- H.P. N.O. — NORMALLY OPEN VALVE, HIGH PRESSURE
- H.P. — NORMALLY CLOSED VALVE HIGH PRESSURE

o encapsulate radioactive krypton.

complete, the vessel is pressurized using both sets of compressors in the High Pressure Room and both cold and hot gas storage (see III-1.2.2.1 for two-gas balanced pressure vessel design); pressure and temperature are maintained throughout the encapsulation period. After encapsula- tion, the vessel is cooled, vented, and evacuated with bellows and cryogenic vacuum pumps (V2 and V3 in Figure III-2). The krypton is returned to the storage cylinders. The vessel is flushed with nitrogen, opened, and the zeolite capsule removed, placed in a shielded storage container, and removed to the Interim Product Storage Room. A fresh zeolite capsule is placed in the vessel and the process repeated.

1.2.2 High Pressure Room. The high pressure room is a special, air-tight, shielded hot cell and contains the high pressure vessel, a removable high pressure barricade with the capability to contain released gas, two assemblies of high pressure compressors (C1 and C2 in Figure III-2 correspond to one assembly), rupture surge tanks (only one shown in Figure III-2), and a set of pumps: a bellows vacuum pump, a cryogenic pump, and a mechanical vacuum pump (V2, V3, and V1, respectively). The mechanical pump is used to activate the sodalite after it is placed in the high pressure vessel before a run and V2 and V3 are used in evacuating the vessel and interconnecting tubing to remove all krypton-85 after a run and before the loaded zeolite is removed from the vessel.

1.2.2.1 High Pressure Vessel. The high pressure vessel uses a balanced pressure concept and a schematic is shown in Figure III-3. The strength-bearing wall of the outer vessel is pressurized with an inert, nonradioactive gas, such as $N_2$ or Ar, to balance the pressure of krypton-85 in the inner vessel. The balancing gas compressor shown in the High Pressure Room is used for the nonradioactive gas and is not shown in Figure III-2. In this concept, the strength-bearing wall of the outer vessel does not become very hot and is not contacted with krypton-85 and its decay product rubidium, thus avoiding potential corrosion. Separate sets of inner vessels could be used to activate one batch of zeolite while another batch is being encapsulated, or the inner vessel could also be final storage container.

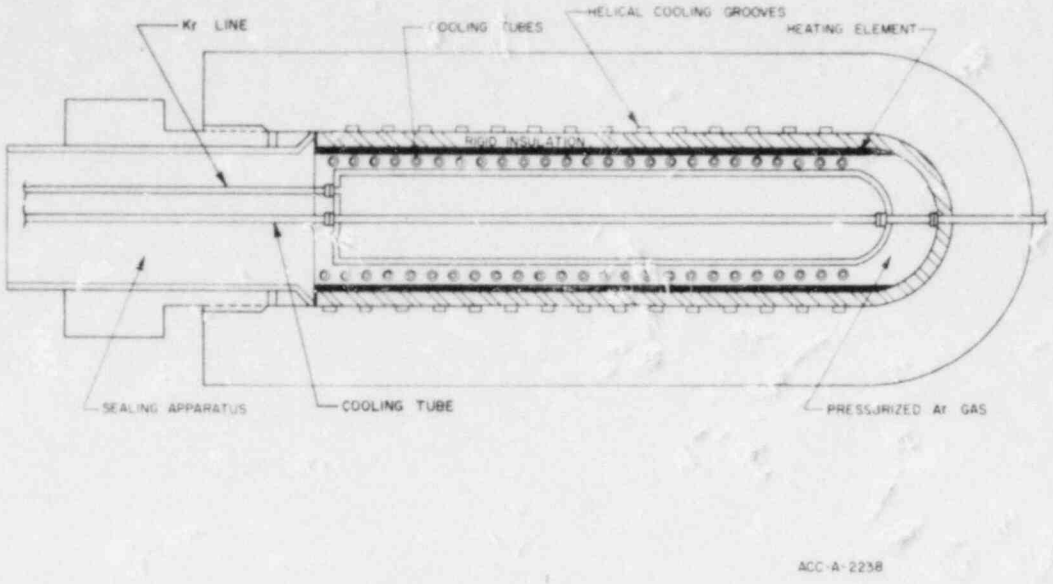


Figure III-3. Schematic of a balanced-gas high pressure vessel used for commercial-scale krypton-85 encapsulation.

Since a large inventory and resulting heat load of krypton-85 can be present during an encapsulation run, calculations were made to estimate maximum steady-state temperatures for various configurations of the inner vessel containing 6% krypton-85 in krypton at 1910 atm (28 000 psi) and sodalite pills.

Equations reported by Yagi and Kunii were selected to determine an effective thermal conductivity for the packed bed of 4 mm diameter by 4 mm long sodalite pills, based on gas thermal conductivity, solid thermal conductivity, void fraction, and other properties.[71]

The SINGLE computer code developed by EG&G Idaho, Inc., was used to perform the heat transfer calculations. Subroutines containing the Yagi and Kunii correlations for calculating the gas properties as a function of temperature and pressure were written to tailor the SINGLE code to the krypton vessel calculations.

The results of the calculations in Table III-II show that the vessel with a 16 cm radius will probably not be acceptable. The temperature gradient during encapsulation is too large, resulting in a centerline temperature of 838°C and a wall temperature of 600°C.

TABLE III-II

CALCULATED STEADY-STATE TEMPERATURES IN VARIOUS DESIGNS OF A KRYPTON-85 ENCAPSULATION VESSEL[x]

| Vessel Type | | | Wall Temperature, °C | Maximum Bed Temperature, °C | Length,[a] m |
|---|---|---|---|---|---|
| Cylinder, Radius, cm | Annulus Radius, cm | | | | |
| | Inner | Outer | | | |
| 16 | -- | -- | 600 | 838 | 0.75 |
| -- | 17[b] | 20 | 20 | 186 | 1.7 |
| -- | 17[b] | 20 | 600 | 638 | 1.7 |
| -- | 12[c] | 20 | 20 | 208 | 0.75 |
| -- | 12[c] | 20 | 100 | 254 | 0.75 |
| -- | 12[c] | 20 | 600 | 644 | 0.75 |

x. Assuming very little convection heat transfer.

a. Length required to give a volume of 58 L for the inner vessel. For a 0.75 m inner vessel, the outer length and diameter are estimated to be about 2.7 and 1.2 m, respectively.

b. Metal rod at center of cylinder.

c. Annular vessel, pressure gas is in contact with center and outside.

A 20 cm-vessel containing a 17-cm radius metal rod would have an acceptable maximum temperature of 638°C during encapsulation. A shorter vessel would be required for similar temperature gradients if the 12-cm radius inner section of the annulus is in contact with the balancing pressure gas, e.g., Ar in Figure III-3.

Transient heat transfer calculations are required to determine cooling times to see if one of these vessel designs is feasible for commercial-scale operations.

These calculations have assumed that most of the heat transfer occurs by conduction and radiation mechanisms and by very little

convection. Thermal currents are induced in the high-pressure gas, and are considered strong enough to require special design of the internal heater shown in Figure III-3 to avoid erosion.[72] Thus, there may be a convective heat transfer mechanism sufficiently strong to lower the steady-state temperature gradient significantly and to allow use of a cylindrical configuration for the inner vessel containing the zeolite and krypton-85. The results shown in Table III-II are conservative and demonstrate that steady-state temperature gradients during encapsulation and after cooling are feasible for large-scale operation.

1.2.2.2 Barricade. While the pressure vessel would be designed to have an extremely low failure probability, a barricade is planned to be placed around the vessel to contain any released krypton-85 gas or vessel fragments. The barricade is estimated to be about 2.4 m inner diameter and about 3.2 m inner height for a 1.2 m diameter by 2.7 m high pressure vessel. The maximum overpressurization in the barricade would not be more than about 4 to 8 atm, in case of failure of the pressure vessel, and the barricade would be designed to contain any released krypton-85. The results of studies using explosives will be used to design an energy-absorbing shielding that would fit over the vessel and inside the barricade.[73,74]

1.2.3 Materials Handling and Intermediate Storage Rooms. Manipulators and an overhead crane are used to transfer zeolites into the vessel and loaded zeolite out of the vessel. Interim storage for 30 days' production of product canisters is provided before shipping to a repository.

1.2.4 Interim Krypton-85 Storage Room. The krypton-85 lag storage is provided for a 30-day production from a reference reprocessing plant scaled to 110% of capacity. The pumping volumes (12 to 18 cylinders) are used for filling and emptying the high pressure vessel.

## 1.3 Preliminary Cost Estimate

The preliminary cost estimate for a Krypton Encapsulation Facility is shown in Table III-III. Although there is a 30% contingency in the total cost, a cost estimate based on a more detailed design could be quite different. Past cost estimates for nuclear facilities have generally increased as the design became more advanced.

TABLE III-III

COST ESTIMATE FOR A COMMERCIAL-SCALE KRYPTON ENCAPSULATION FACILITY[a]

| Description | Total Cost[b] ($1000) |
|---|---|
| **Facitity Costs** | |
| Design and Project Management | $ 587 |
| Utilities and Equipment | 449 |
| Material for Building | 418 |
| Labor for Building | 219 |
| Indirect Costs | 217 |
| Subtotal | 1,890 |
| Escalation | 680 |
| Contingency | 830 |
| Total Construction Cost | 3,400 |
| **Process Equipment Costs** | |
| Design | 135 |
| Two-gas, Balanced Pressure Vessel, Remotely Operated (58L Volume) | 193 |
| Vessel Barricade | 72 |
| Two Compressors | 100 |
| Vacuum Pumps | 13 |
| Cranes/Manipulators/TV Monitors | 100 |
| Valves, Tubine, Fittings, Regulators | 37 |
| Instrumentation, Control Board | 35 |
| Lab Equipment | 92 |
| Installation | 85 |
| Subtotal | 861 |
| Contingency | 258 |
| Total | 1,120 |
| Total Facility Costs | 4,520 |

a. Capacity is 18.7 MCi/yr.

b. First quarter 1979 dollars.

If some extra equipment items such as a high pressure vessel or compressors need to be on hand for quick replacement, the resulting additional cost can be estimated from Table III-III.

## 1.4 Safety Considerations

Due to the large inventory of krypton-85 that could be in the high pressure vessel (less than 1.4 MCi, assuming 58L and a total void fraction of 0.7), the vessel must be designed with a large safety margin. The barricade would provide a secondary containment to the krypton-85, and if necessary, the high pressure room a tertiary containment.[75] A detailed safety assessment of the vessel, barricade, and high pressure room needs to be made to demonstrate an extremely low probability for significant krypton-85 release. A safety assessment is also required for containing several megacuries of krypton-85 in the lag storage area, transfer lines, and immobilized product handling and interim storage areas.

Since in any commercial-scale krypton-85 immobilization facility, a large inventory of several megacuries could be present as lag storage due to differences in processing schedules between the recovery and immobilization facilities or to possible immobilization process upsets, the large krypton inventory in the high pressure vessel during encapsulation may not add significantly to the facility containment requirements. An assessment of krypton release probabilities from all sources must be made in each candidate immobilization facility before any detailed comparisons can be made.

# IV. CONCLUSIONS

This report demonstrates that krypton-85 encapsulation is technically and economically feasible as a krypton immobilization process. Krypton from a 2000 MTHM per year commercial reprocessing plant can be encapsulated in unleached sodalite at a rate faster than one batch per day at 575°C and 1630 atm, giving a product containing 20 to 26 $cm^3$ Kr at STP per gram. The resulting leakage rate of encapsulated Kr at a storage temperature of 150°C was measured for one year to be as low as <0.1% in ten years. Mixtures of krypton-xenon up to about 50% xenon can be used to give krypton loadings in sodalite which are only about 15% lower than with pure krypton. The small quantities of xenon that are encapsulated were found to slow krypton leakage rates even further. The rate of encapsulating krypton from krypton-xenon mixtures needs to be measured further in order to establish the limits of added xenon composition that will give 20 $cm^3/g$ loading at a one batch per day operation. Preliminary results at 500°C indicate that a 70/30 Kr/Xe mixture can also be encapsulated at 20 $cm^3/g$ in one batch per day at 575°C.

The design and cost estimates for an encapsulation facility for a commercial-scale reprocessing plant do not show any major problems in a lack of available technology or in any excessive costs. High-pressure technology has been used in larger scale for the chemical industry, sometimes with highly reactive chemicals. With krypton-85, the gas is inert with no mechanisms for runaway explosions, and the pressure vessel can be designed for a high safety level.

Some of the further work is required in the following:

(1) Determine the added xenon levels that still allow 20 cc/g Kr loading at approximately one run per day.

(2) Measure leakage rates at potential storage temperatures (100 to 200°C) for ten years to verify the predictions from one-year measurements.

(3) Measure long-term leakage rates of krypton-85 encapsulated in sodalites.

(4) Determine standards for manufacturing the sodalite with the preferred loading and leakage characteristics.

(5) Develop a more detailed design of the commercial-scale encapsulation facility and perform a preliminary safety analysis of the process.

## REFERENCES


1. National Council on Radiation Protection and Measurements, Krypton-85 in the Atmosphere -- Accumulation, Biological Significance and Control Technology, NCRP Report No. 44, Washington, D.C. (July 1, 1975).

2. D. A. Knecht and R. A. Brown, "Strategy Analysis for Krypton-85 Waste Management," Trans. ANS, to be published 1979.

3. P. J. Mellinger, G. R. Hoenes, L. W. Brackenbush, and J. Greenborg, $^{85}$Kr Management Trade-offs: A Perspective to Total Radiation Dose Commitment. To be published, Battelle, Pacific Northwest Laboratories.

4. "Environmental Radiation Protection Standards for Nuclear Power Operation," Federal Register, 42, No. 9, Part VII, 2858 (January 13, 1977).

5. Alternatives for Managing Wastes from Reactors and Post-Fission Operations in the LWR Fuel Cycle, ERDA-76-43, Chapt. 14.1, Vol. 2, 14.1-14.7 (April 1976).

6. W. S. Diethorn, and W. L. Stockho, "The Dose to Man from Atmospheric $^{85}$Kr", Health Physics, 23, 653 (1972).

7. D. E. Bernhardt, A. A. Moghissi, and J. A. Cochran, "Atmospheric Concentration of Fission Product Noble Gases," Noble Gases CONF-750915, R. E. Stanley, and A. A. Moghissi, editors, (1974).

8. K. Telegadas and G. J. Ferber, "Atmospheric Concentration and Inventory of $^{85}$Kr in 1973," Science 190, 882-883 (November 28, 1975).

9. U.S. DOE Effluent Information System, operated by EG&G Idaho, Inc.

10. C. L. Bendixsen and G. F. Offutt, Rare Gas Recovery Facility at the Idaho Chemical Processing Plant, IN-1221 (April 1968).

11. C. L. Bendixsen and F. O. German, Operation of the ICPP Rare Gas Recovery Facility During Fiscal Year 1970, ICP-1001 (October 1971).

12. C. L. Bendixsen et al., 1972 Operation of the ICPP Rare Gas Recovery Facility, ICP-1023 (March 1973).

13. C. L. Bendixsen and F. O. German, 1974 Operation of the ICPP Rare Gas Recovery Facility, ICP-1057 (March 1975).

14. T. R. England et al., "ENDF/B-V Yields," Applied Nuclear Data Research and Development, LA7596PR (December 1978).

15. Management of Commercially Generated Radioactive Waste, Draft Environmental Impact Statement, DOE/EIS-0046-D (April 1979).

16. Nuclear Quick Reference II, GED-5542B, Nuclear Energy Group, General Electric Corp., San Jose, CA, (1979).

17. 40CFR190 Environmental Radioactive Protection Requirements for Normal Operations of Activities in the Uranium Fuel Cycle, Final Environmental Statement, EPA 520/4-76-016 (November 1976).

18. Preliminary Safety Analysis Report, Nuclear Fuel Recovery and Recycle Center. Exxon Nuclear Company, Inc., XN-FR-32, NRC Docket Number 50-564 (1976).

19. Design Integration Study. Spent LWR Fuel Recycle Complex. Conceptual Design Case A-1, Separated Streams, DP-CFP-78-121 (November 1978).

20. C. L. Bendixsen and D. A. Knecht, "Separation and Storage of Krypton," Proceedings of the International Symposium on the Management of Wastes from the LWR Fuel Cycle, CONF-760701, 343 (1976).

21. C. M. Slansky, "Separation Processes for Noble Gas Fission Products from the Off-Gas of Fuel-Reprocessing Plants," At. En. Rev., 9, 423 (1971).

22. R. H. Rainey et al., Completion Report: Evaluation of the Use of Permselective Membranes in the Nuclear Industry for Removing Radioactive Xenon and Krypton from Various Oxygen Streams, ORNL-4522 (1971).

23. M. J. Stephenson et al., ORGOP Selective Adsorbtion Pilot Plant for Decontamination of Fuel Reprocessing Plant Off-Gas, K-1876 (1977).

24. Technology for Commercial Radioactive Waste Management, DOE/ET-0028, Vols. 2 and 3 (May 1979).

25. W. O. Burch et al., Retention of Gaseous Fission Products in LMFBR Fuels, IAEA-Ag-63-2 (1976).

26. D. A. Knecht, An Evaluation of Methods for Immobilizing Krypton-85, ICP-1125 (July 1977).

27. B. A. Foster and D. T. Pence, An Evaluation of High Pressure Steel Cylinders for Fission Product Noble Gas Storage, ICP-1044 (February 1975).

28. T. R. Pinchback, Materials Screening Tests for the Krypton-85 Storage Development Program, TREE-1291 (January 1979).

29. G. L. Tingey et al., Entrapment of Krypton in Sputter Deposited Metals -- A Storage Medium for Radioactive Gases, PNL-2879 (January 1979).

30. J. A. Van Vechten, R. J. Gambino and J. J. Cuomo, "Encapsulation of Radicactive Noble Gas Waste in Amorphous Alloy," IBM J. Res, Develop., 23, 278-285 (May 1979).

31. C. W. Nielsen, Safety Analysis Report for Packaging Krypton Shipping Container, ICP-1077 (June 1975).

32. R. W. Benedict, An Evaluation of Methods for Immobilizing Solids Loaded with Krypton-85, ICP-1130 (August 1977).

33. N. Bartlett, "Xenon Hexafluoroplatinate (V), $Xe^{+}(PtF_6)^{-}$" Proc. Chem. Soc. 1962, 218.

34. B. A. Stables and D. T. Pence, An Evaluation of Quinol Clathrate for Fission Product Noble Gas Storage, ICP-1045 (July 1974).

35. J. W. McBain, The Sorption of Gases and Vapors by Solids (London: Rutledge and Sons, 1932).

36. R. M. Barrer, "Separation of Mixtures Using Zeolites as Molecular Sieves. Part 1. Three classes of Molecule-Sieve Zeolite," J. Soc. Chem. Ind., 64, 130-131 (1945).

37. D. W. Breck, Zeolite Molecular Sieves (New York: John Wiley & Sons, 1974).

38. R. M. Barrer, Zeolites and Clay Minerals as Sorbents and Molecular Sieves (New York: Academic Press, 1978).

39. W. J. Sesny and L. H. Shaffer, Fluid Encapsulation Product, U.S. Patent 3,316,691 (May 2, 1967).

40. D. Fraenkel and J. Shabtai, "Encapsulation of Hydrogen in Molecular Sieve Zeolites," J. Amer. Chem. Soc., 99, 7074-76 (1977).

41. R. M. Barrer and D. E. W. Vaughan," Trapping of Inert Gases in Sodalite and Cancrinite Crystals, J. Phys. Chem. Solids, 32, 731-743 (1971).

42. G. A. Cook, Helium and the Rare Gases, Vol. 1 (New York: Interscience, 1961) p. 228.

43. V. Schreyer, H. S. Yoder, and L. T. Aldrich, Yearbook 1959-60, Carnegie Institute, Washington, Vol. 59, p. 94.

44. D. E. W. Vaughan, Encapsulation of Rare Gases, (PhD. Thesis, Imperial College, London, 1967).

45. R. M. Barrer and D. E. W. Vaughan, "Sorption and Diffusion of Rare Gases in Heulandite and Stilbite," Surface Science, 14, 77-92 (1969).

46. R. M. Barrer and D. E. W. Vaughan, "Trapping and Diffusion of Rare Gases in Phillipsite, Zeolite K-M and other Silicates," Trans. Faraday Society, 67, 2129-2136 (1971).

47. R. M. Barrer and R. Papadopoulos, "The Sorption of Krypton and Xenon in Zeolites at High Pressures and Temperatures," Proc. Roy. Soc. Lond. A, 326, 315-330 (1972).

48. R. A. Brown, M. Hoza, and D. A. Knecht, "$^{85}Kr$ Storage by Zeolite Encapsulation," Proc. Fourteenth ERDA Air Clean, Conf., 1976, CONF-760822, Vol. 1, pp. 118-131 (February 1977).

49. S. Brunauer, The Adsorption of Gases and Vapors (Princeton: Princeton University Press, 1943).

50. J. Crank, The Mathematics of Diffusion (Oxford: Clarendon Press, 1975).

51. H. S. Carslow and J. C. Jaeger, Conduction of Heat in Solids, (Oxford: Clarendon Press, 1959).

52. R. M. Barrer, Diffusion in and Through Solids, (Cambridge: Cambridge University Press, 1941; Ann Arbor: Xerox University Microfilms, 1975).

53. R. M. Barrer, "Intracrystalline Diffusion," Molecular Sieve Zeolites II, Adv. Chem. Ser. 102, (Washington, D.C.: American Chemical Society, 1971).

54. P. L. Walker, L. C. Austin, and S. P. Nandi, "Activated Diffusion of Gases in Molecular-Sieve Materials," Chem. Phys. of Carbon, 2, 257-371 (1966).

55. R. M. Barrer and D. E. W. Vaughan, "Solution and Diffusion of Helium and Neon in Tridymite and Cristobalite," Trans. Faraday Soc., 63, 2275-90 (1967).

56. D. M. Ruthven and R. I. Derrah, "Diffusion of Monatomic and Diatomic Gases in 4A and 5A Zeolites," J. Chem. Soc. Faraday Trans. 1, 71, 2031-2044 (1975).

57. D. M. Ruthven and R. I. Derrah, "A Comparative Study of the Diffusion of $C_2H_6$, $C_2H_4$, and n-$C_8H_{12}$ in Erionite and in Type A Zeolite," J. Coll. Interf. Sci., 52, 399-403 (1975).

58. A. Kusa, and I. J. Ohgushi, "Application of Percolation Theory to Ion-Exchanged Molecular Sieves A," J. Phys. Chem. Solids, 38, 1233-1236 (1977).

59. D. M. Ruthven, "Diffusion in Molecular Sieves" A Review of Recent Developments," Molecular Sieves II, ACS Symposium Ser., 40, (Washington, D.C.: American Chemical Society, 1977), pp. 320-333.

60. K. Pilchowski, F. Danes, and F. Wolf," Determination of Diffusion in Solids from Adsportion Data, II. Effects of Sorption Induced Concentration Changes in the External Phase on the Sorption Rate," Kolloid-Z.Z. Poly. 230, 328-336 (1969).

61. R. M. Barrer and B. E. Fender, "The Diffusion and Sorption of Water in Zeolites. I. Sorption," J. Phys. Chem. Solids, 21, 1-11 (1961).

62. R. M. Barrer and B. E. Fender, "The Diffusion and Sorption of Water in Zeolites II. Intrinsic and Self-Diffusion," J. Phys. Chem. Solids, 21, 12-24 (1961).

63. C. N. Satterfield and A. J. Frabetti, "Sorption and Diffusion of Gaseous Hydrocarbons in Synthetic Mordenite," AIChE Journal, 13, 731-738 (1967).

64. W. W. Brandt and W. J. Rudloff, "Rapid Sorption Processes on Granular Zeolites," J. Phys. Chem. Solids, 25, 167-176 (1964).

65. W. W. Brandt and W. J. Rudloff, "Gaseous Diffusion in a Natural Zeolite in Relation to Crystalline Disorder," Z. Phys. Chem. (Frankfort), 42, 201-210 (1964).

66. P. E. Eberly, "Diffusion Studies in Zeolites and Related Solids by Chromatographic Techniques," Ind. Eng. Chem. Fund 8, 25-30 (1969).

67. K. Fiedler and D. Gelbin, "Model for Analyzing Diffusion in Zeolite Crystals," J. Chem. Soc. Faraday Trans. 1, 10, 2423-2433 (1978).

68. D. M. Ruthven and K. F. Loughlin, "The Sorption and Diffusion of n-Butane in Linde 5A Molecular Sieve," Chem. Eng. Sci. 26, 1145-1154 (1971).

69. N. E. Bibler, Radiolytic Gas Production from Tritiated Water Sorbed on Molecular Sieves, DPST-77-375 (July 1977).

70. R. M. Barrer and J. F. Cole, "Interaction of Sodium Vapor with Synthetic Sodalite: Sorption and Formation of Color Centers," J. Phys. Chem. Solids, 29, 1755-1758 (1968).

71. S. Yagi and D. Kunii, "Heat Transfer Characteristics of Porous Rocks," AIChE J., 6, 71-8 (March 1960).

72. C. H. Curtis and H. A. Pohto, "Design Aspects of A Multiwall 1750°C Furnace for 20,000 Psi Argon Operation," Am. Soc. of Mechanical Engineers Pressure Vessel and Piping Nuclear Conference, CONF-740606-1 (June 24-28, 1974).

73. J. F. Proctor, Structural Analysis of NOL Explosive Testing Facilities, NOLTR-69-84 (April, 1969).

74. R. L. Porter, P. A. Lobo, and C. M. Sliepcevich, "Design and Construction of Barricades," Ind. Eng. Chem., 48, 841 (May, 1956).

75. N. J. Swanson et al., "Preliminary Design of the Hot Fuel Examination Facility (HFEF)," Proceedings of the 17th Conference on Remote Systems Technology, American Nuclear Society, pp. 131-139 (November 1969).

# APPENDIX A

## KRYPTON-XENON PROPERTIES

# APPENDIX A

## KRYPTON-XENON PROPERTIES

This appendix gives information about the following properties of krypton, xenon, and krypton-xenon mixtures:

(1) Isotopic composition

(2) Decay heat output

(3) Equation of state

(4) Thermal conductivity.

These properties are required for zeolite encapsulation and storage process development and design work, such as in calculating krypton and xenon inventories, sizing equipment, estimating heating and cooling requirements, and performing detailed modeling.

Isotopic distribution of krypton and xenon formed in $^{233}U$, $^{235}U$, and $^{239}Pu$ fission are shown in Table A-I.[1,2] A four-year irradiation time in the reactor and a zero- and 1.5-year cooling time before reprocessing is assumed.

$$N = N_o \cdot \exp(-0.0646 \cdot t) \qquad \text{(A-1)}$$

Krypton-85 has a 10.73-year half-life, with the number of moles N remaining after t years from the initial number of moles of krypton-85, $N_o$. Figure A-1 shows the decay scheme and end-point energies for $^{85}Kr$. The average energy per decay is 0.246 MeV and the decay heat output, $E_d$, for 7.8% $^{85}Kr$ in krypton is

$$E = 48.33\ N_o \cdot \exp(-0.0646 \cdot t) \qquad \text{(A-2)}$$

where $E_d$ is in watts.[3] Figures A-2 and A-3 show the $^{85}Kr$ heat generation rate as a function of time for 6 to 8% $^{85}Kr$ in krypton.

TABLE A-I

FISSION PRODUCT NOBLE GAS COMPOSITION IN ATOM PERCENT[a]

| | Krypton Atom % Directly Out of Reactor | | | | | Xenon Atom % | | |
|---|---|---|---|---|---|---|---|---|
| | $^{83}Kr$ | $^{84}Kr$ | $^{85}Kr$ | $^{86}Kr$ | $^{131}Xe$ | $^{132}Xe$ | $^{134}Xe$ | $^{136}Xe$[b] |
| Thermal Fission | | | | | | | | |
| $^{233}U$ | 16.90 | 28.28 | 7.37 | 47.45 | 13.08 | 17.91 | 22.89 | 46.12 |
| $^{235}U$ | 14.30 | 26.55 | 6.60 | 52.55 | 10.61 | 15.81 | 28.68 | 44.90 |
| $^{239}Pu$ | 17.96 | 28.86 | 6.95 | 46.22 | 12.64 | 17.73 | 25.05 | 44.59 |
| Fast Fission | | | | | | | | |
| $^{233}U$ | 16.97 | 28.00 | 7.51 | 47.52 | 13.53 | 17.93 | 22.51 | 46.01 |
| $^{235}U$ | 15.10 | 27.10 | 6.73 | 51.07 | 11.60 | 16.97 | 27.50 | 44.11 |
| $^{239}Pu$ | 18.25 | 28.88 | 7.06 | 45.82 | 12.77 | 17.53 | 24.34 | 45.35 |
| | Krypton Atom % After 1.5-Year Cool Time | | | | | | | |
| Thermal Fission | | | | | | | | |
| $^{233}U$ | 17.01 | 28.47 | 6.74 | 47.78 | 13.08 | 17.91 | 22.89 | 46.12 |
| $^{235}U$ | 14.39 | 26.72 | 6.02 | 52.87 | 10.61 | 15.81 | 28.68 | 44.90 |
| $^{239}Pu$ | 18.08 | 29.05 | 6.35 | 46.52 | 12.64 | 17.73 | 25.05 | 44.59 |
| Fast Fission | | | | | | | | |
| $^{233}U$ | 17.09 | 28.20 | 6.86 | 47.85 | 13.53 | 17.93 | 22.51 | 46.01 |
| $^{235}U$ | 15.20 | 27.26 | 6.14 | 51.39 | 11.60 | 16.97 | 27.50 | 44.11 |
| $^{239}U$ | 18.37 | 29.06 | 6.45 | 46.12 | 12.77 | 17.53 | 24.34 | 45.35 |

a. Assumes four-year irradiation time.

b. Assumes 90% conversion of $^{135}Xe$ to $^{136}Xe$ by neutron capture.

State equations were developed for krypton and xenon using available data modeled to the Redlich-Kwong equation[4,5]

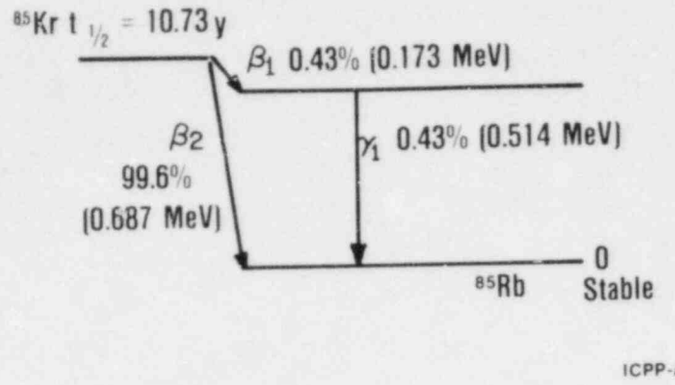


Figure A-1. Decay scheme and end-point energies for krypton-85.

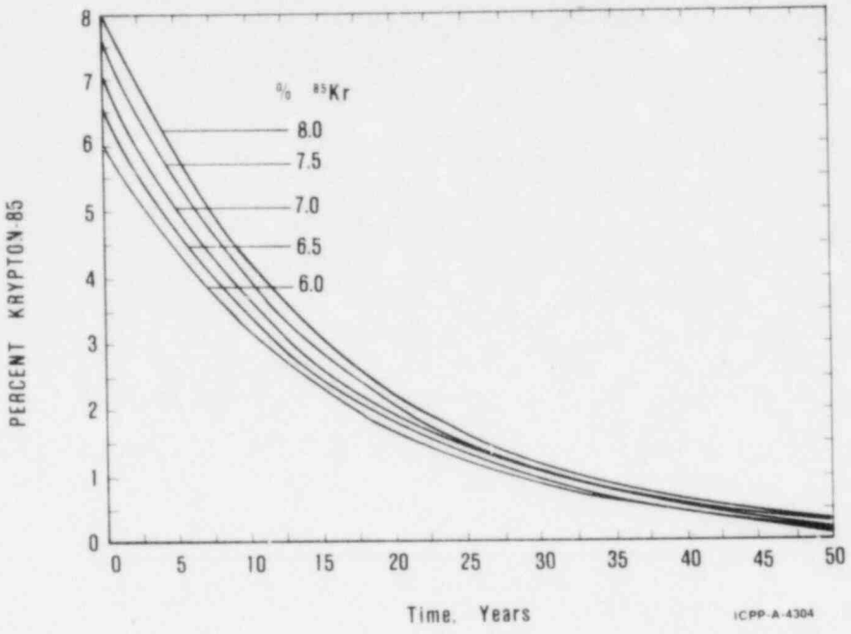


Figure A-2. Percent of krypton-85 in krypton as a function of time for various initial concentrations.

$$P = \frac{R}{v - b} - \frac{a}{v(v + b)} \qquad \text{(A-3)}$$

where P is the pressure in atmospheres, v is the specific volume in $cm^3 mole^{-1}$, T is the absolute temperature in Kelvin, R is the ideal gas constant, and a and b are constants. Using the available data for krypton,[6,7,8] a and b are:

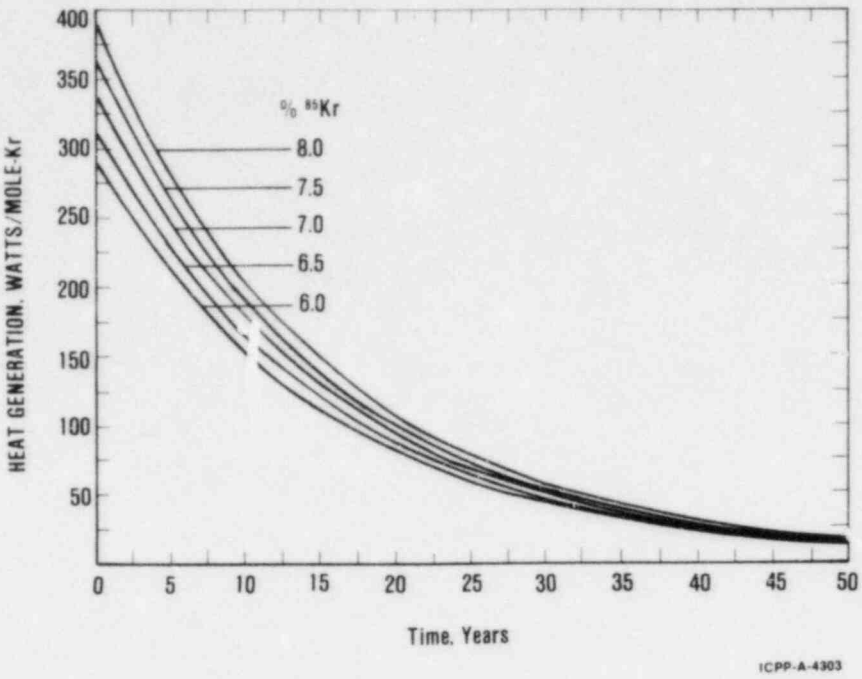


Figure A-3. Heat generation rates of krypton-85 as a function of time for various initial concentrations.

$$b_{Kr} = 28.207 - 1.0485 \times 10^{-4} T \quad \text{(A-4)}$$

$$a_{Kr} = RT(-28.153 + 6487.6/T + 5452723.6/T^2 + b_{Kr} \quad \text{(A-5)}$$

Data for xenon[9,10,11] gave the following values of a and b:

$$a_{Xe} = RT(-75.243 + 74268.7/T) \quad \text{(A-6)}$$

$$b_{Xe} = 35.673 \quad \text{(A-7)}$$

These correlations are good in the ranges 25 to 525°C and 0 to 2000 atm, with average and maximum errors in the data of less than 2 and 6%, respectively.

Figures A-4 and A-5 show compressibility isotherms calculated from the Redlich-Kwong equation as a function of pressure for krypton and xenon, respectively. For krypton-xenon mixtures, the mixture parameters $b_n$ and $a_n$ must be estimated by using the pure gas parameters (Equations A4 through A7) and mole fractions $y_i$ in the following mixing rules:[12]

$$b_n = b_{Kr}\, y_{Kr} + b_{Xe}\, y_{Xe} \quad \text{(A-8)}$$

$$a_n = a_{Kr}\, y_{Kr} + a_{Xe}\, y_{Xe} + a_{Kr\cdot Xe}\, y_{Kr}\, y_{Xe} \qquad \text{(A-9)}$$

$$a_{Kr\cdot Xe} = (a_{Kr} \cdot a_{Xe})^{1/2} \qquad \text{(A-10)}$$

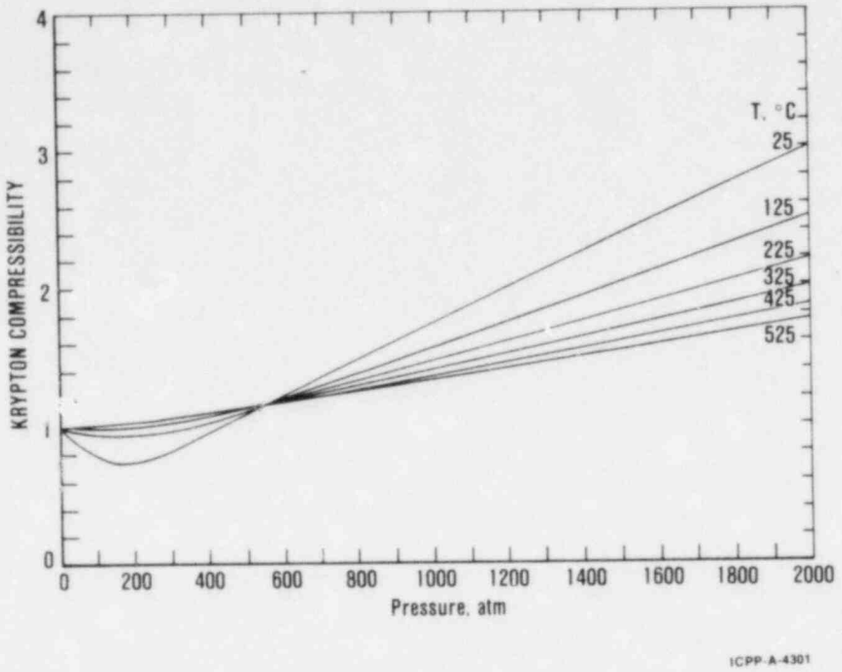


Figure A-4. Krypton compressibility isotherms as a function of pressure.

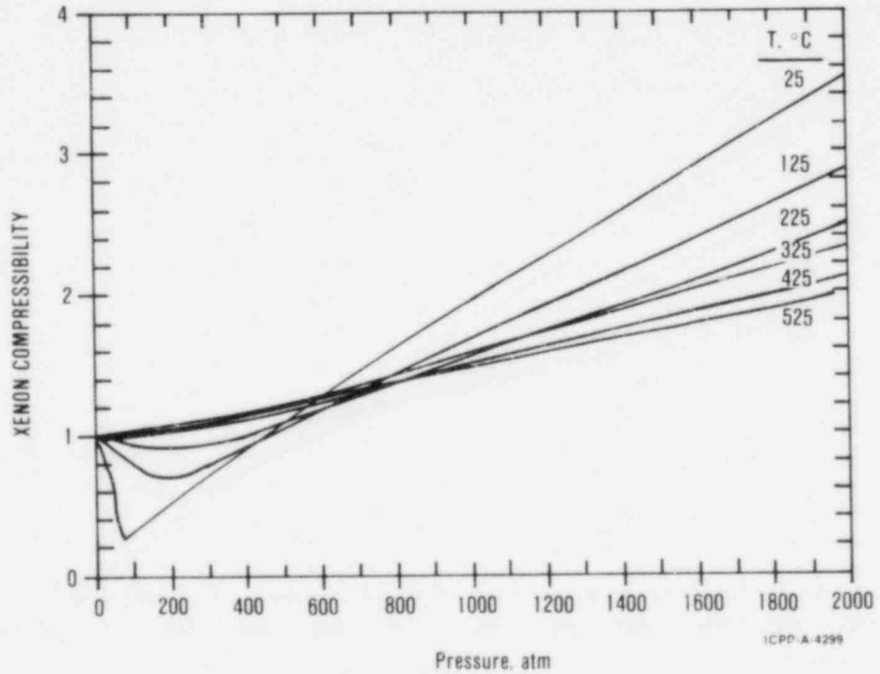


Figure A-5. Xenon compressibility isotherms as a function of pressure.

These rules produce good results for noble gas mixtures. The heat capacity may be estimated with the Redlich-Kwong equation by using the following relationships[13]

$$C_v - C_{vo} = T \int_{\infty}^{v} \left(\frac{\partial^2 P}{\partial T^2}\right) \Big|_v dv \qquad \text{(A-11)}$$

where $C_v$ and $C_{vo}$ are the real and ideal constant volume heat capacities in calories·mole$^{-1}$·K$^{-1}$. The constant pressure heat capacity is found using the following

$$C_p = C_v + T \left(\frac{\partial P}{\partial T}\right)_v \left(\frac{\partial V}{\partial T}\right)_p \qquad \text{(A-12)}$$

Gas thermal conductivities were modeled using available literature data. A model expressing both the temperature and pressure dependence of the thermal conductivity was chosen[14,15]

$$k = k_o + \gamma_1 v^{\gamma_2} \qquad \text{(A-13)}$$

where k and $k_o$ are the high- and low-pressure thermal conductivities, in W-cm$^{-1}$-K$^{-1}$, v is the gas volume, in cm$^3$-mole$^{-1}$, and $\gamma_1$ and $\gamma_2$ are parameters. Krypton and xenon equations for $k_o$ are given below[16]

$$k_o = 1.993 \times 10^{-5} + 2.65 \times 10^{-7} \cdot T - 3.72 \times 10^{-11} \cdot T^2 \qquad \text{(A-14)}$$

$$k_o = 1.161 \times 10^{-5} + 1.736 \times 10^{-7} \cdot T - 2.41 \times 10^{-11} \cdot T^2 \qquad \text{(A-15)}$$

The parameters $\gamma_1$ and $\gamma_2$ were found for krypton[17,18]

$$\gamma_1 = 3.472 \times 10^{-2} \qquad \text{(A-16)}$$

$$\gamma_2 = -1.212 \qquad \text{(A-17)}$$

Since adequate data for xenon was not available, the correlation developed in Owens and Thodos[15] was used. Figures A-6 and A-7 show thermal conductivity isotherms as a function of pressure for krypton and xenon, respectively. Mixture rules have been developed for thermal conductivity. The Wassiljewa equation is generally used for this purpose[14]

$$k_m = \left[\frac{k_1}{1.0 + A_{12}\left(\frac{y_2}{y_1}\right)}\right] + \left[\frac{k_2}{1.0 + A_{21}\left(\frac{y_1}{y_2}\right)}\right] \qquad \text{(A-18)}$$

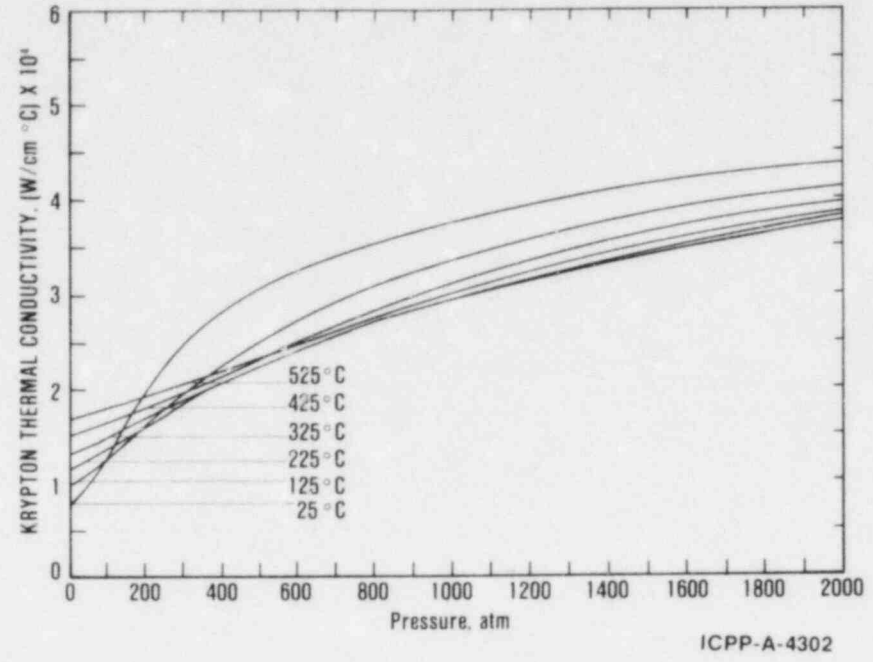


Figure A-6. Krypton thermal conductivity isotherms as a function of pressure.

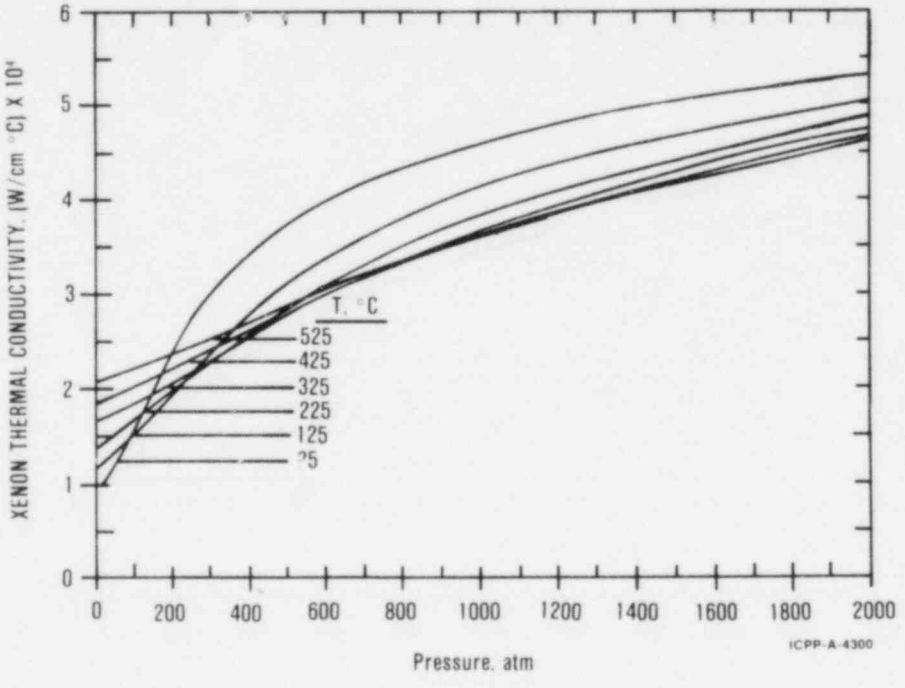


Figure A-7. Xenon thermal conductivity isotherms as a function of pressure.

where $k_1$, $k_2$, and $k_m$ are the krypton, xenon, and mixture thermal conductivities, $y_1$ and $y_2$ are gas mole fractions, and $A_{12}$ and $A_{21}$ are given by

$$A_{12} = 0.294 \left[ 1.0 + 0.894 \left( \frac{k_1}{k_2} \right)^{1/2} \right]^2 \qquad \text{(A-19)}$$

$$A_{21} = 0.235 \left[ 1.0 + 1.1119 \left( \frac{k_2}{k_1} \right)^{1/2} \right]^2 \qquad \text{(A-20)}$$

## REFERENCES


1. T. R. England et al., "ENDF/B-V Yields," Applied Nuclear Data Research and Development, LA7596PR (December 1978).

2. F. L. Lisman et al., "Fission Yields and Branching Ratios of Krypton-85 in Thermal Neutron Fission of Uranium-235, Plutonium-239, and Plutonium-241," J. Inorg. Nucl. Chem., 33, 643-649 (1971).

3. National Council on Radiation Protection and Measurements, Krypton-85 in the Atmosphere -- Accumulation, Biological Significance and Control Technology, NCRP Report No. 44, Washington, D.C. (July 1, 1975).

4. K. K. Shaw and G. Thodos, "A Comparison of Equations of State," Ind. Eng. Chem., 57, 30-37 (1965).

5. R. Simonet and E. Behar, "A Modified Redlich-Kwong Equation of State for Accurately Representing Pure Components Data," Chem. Eng. Sci., 31, 37-43 (1976).

6. N. J. Trappeniers, T. Wassenaar, and G. J. Walkers, "Isotherms and Thermodynamic Properties of Krypton between 0° and 150°C and at Densities up to 620 Amagats," Physica, 32, 1503-20 (1966).

7. J. A. Beattie, J. S. Brierley, and R. J. Barriault, "The Compressibility of Gaseous Krypton II. The Virial Coefficients and Potential Parameters of Krypton," J. Chem. Phys., 20, 1615-18 (October 1952).

8. E. Whalley, Y. Lupien, and W. G. Schneider, "Compressibility of Gases VIII. Krypton in the Temperature Range 0° to 600°C and Pressure Range 10-80 Atm," Trans. ASME, 76, 1001-04 (August 1954).

9 J. A. Beattie, R. J. Barriault, and J. S. Brierley, "The Compressibility of Gaseous Xenon II. The Virial Coefficients and Potential Parameters of Xenon," J. Chem. Phys., 19, 1222-26 (1951).

10. E. Whalley, Y. Lupien, and W. G. Schneider, "The Compressibility of Gases at High Temperatures X. Xenon in the Temperature Range 0° to 700°C and the Pressure Range 8 to 50 Atm." Can. J. Chem., 33, 633-36 (1955).

11. A. Michels, T. Wassenaar, and P. Louwerse, "Isotherms of Xenon at Temperatures between 0° and 150°C and at Densities up to 515 Amagats," Physica, 20, 99-106 (1954).

12. J. B. Prausnitz, Molecular Thermodynamics (New York: McGraw-Hill, 1968).

13. N. A. Hall and W. E. Ibele, Engineering Thermodynamics (Englewood Cliffs, N.J.: Prentice-Hall, 1960).

14. R. C. Reid and T. K. Sherwood, The Properties of Gases and Liquids, 2nd Ed. (New York: McGraw-Hill, 1966).

15. E. J. Owens and G. Thodos, "Thermal Conductivity-Reduced-State Correlation for the Inert Gases," AIChE Journal, 3, 454-61 (December 1957).

16. V. K. Saxena and S. C. Saxena, "Thermal Conductivity of Krypton and Xenon in the Temperature Range 350-1500 K," J. Chem. Phys., 51, 3361-68 (October 1969).

17. R. Tufeu, B. LeNiendre, and P. Burg, "High Pressure Thermal Conductivity of Krypton," J. Acad. Sci. Paris, B273, 61-64 (1971).

18. F. G. Keyes, "Thermal Conductivity of Gases," Trans. ASME, 7, 1395-96 (November 1955).

# APPENDIX B

# ZEOLITE MATERIAL CHARACTERIZATION

# APPENDIX B

## ZEOLITE MATERIAL CHARACTERIZATION

The basic sodalite (sodalite hydrate or hydroxy sodalite) used in this program is a synthetic sodium aluminosilicate zeolite. The chemical formula for the pure material is[1]

$$Na_6(AlO_2)_6(SiO_2)_6xH_2O \quad \text{or}$$
$$Na_2O:Al_2O_3:2SiO_2:xH_2O.$$

The fundamental units of this material, and all zeolites, are $SiO_4$ and $AlO_4$ tetrahedra linked together through the oxygen atoms. All oxygen atoms are shared by two adjoining tetrahedra, so that there are no unshared oxygens in the framework. The $SiO_4$ and $AlO_4$ tetrahedra alternate in the framework with no Si-O-Si or Al-O-Al bonds. Each Al atom causes a net negative charge in the framework that is balanced by a cation, sodium, in the sodalite case. The framework topology for sodalite is a truncated octahedron (14-hedron Type I) with eight of the 6-rings, six of the 4-rings, and 24 vertices. The structure of nine linked octahedra with a krypton model occupying one of them is shown in Figure B-1. According to Breck[1], the polyhedra of sodalite is distorted so that the arrangement of the oxygen atoms is not regular. The size of the free aperture in the 6-rings is 2.2A and the inscribed sphere has a diameter of about 6.6A in the hydrated material. The sodium cations are near the 6-rings, but in the cage along with several water molecules. On dehydration, the sodium ions probably move into the 6-rings.

During the synthesis of sodalite, extraneous sodium hydroxide can be incorporated into the structure. The position of the sodium ions of this intercalated material will be similar to the structural sodiums, i.e., near the 6-rings in hydrated material. The extraneous hydroxyl ions will be in the cages. As the amount of intercalated

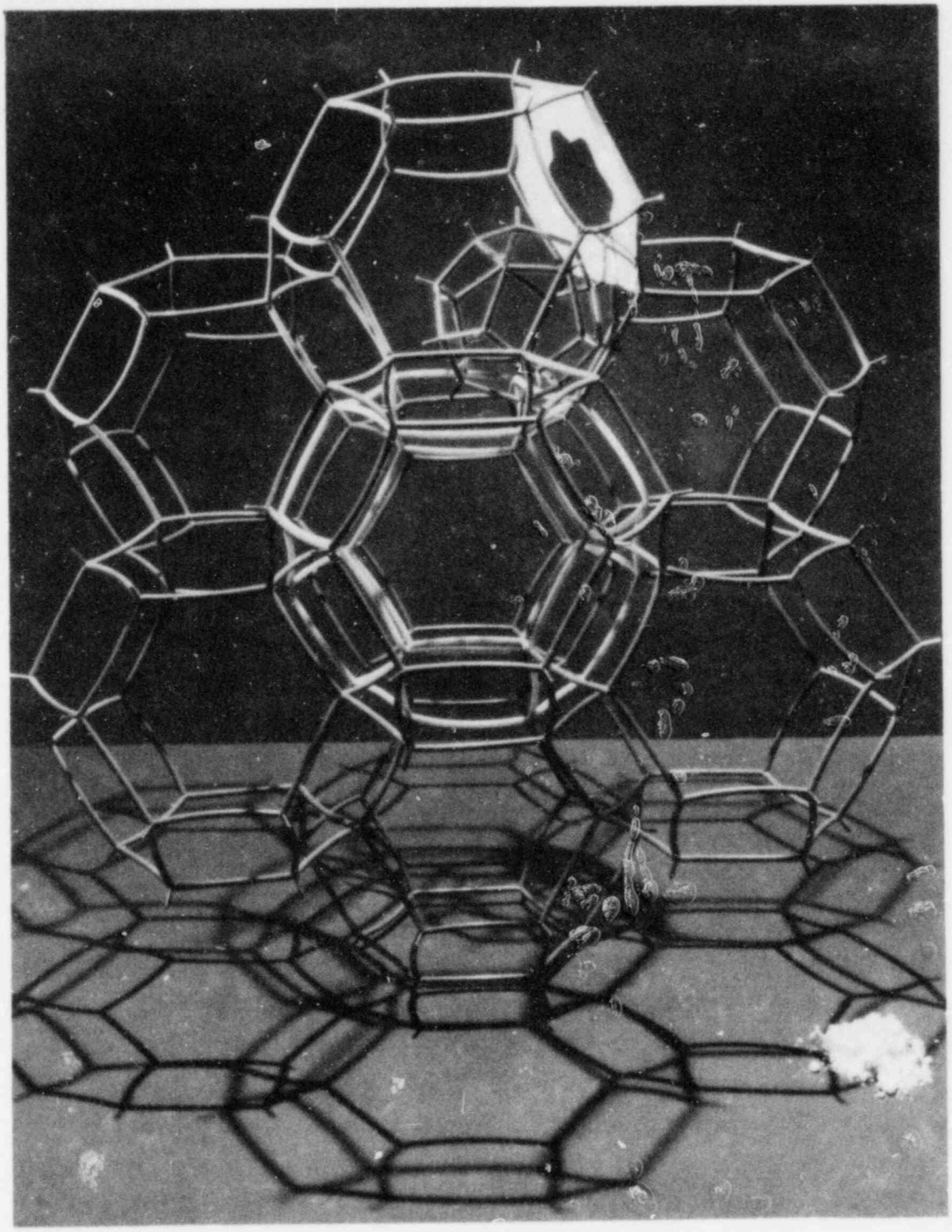

Figure B-1. Model of sodalite cages. Relative cage opening shown in upper right of cage containing model of krypton atom.

sodium hydroxide increases, the capacity to take up water decreases, since the free volume inside the cages is fixed. The additional

sodiums will block more windows making diffusion into and out of the cages by other molecules more difficult. If sufficient additional sodium hydroxide molecules are present, no diffusion into the cages will occur.[2] The intercalcated sodium hydroxide can be removed to different extents by washing with water.

In addition to the intercalated sodium hydroxide, there is the possibility that $SiO_2$ may form as a separate phase during synthesis and be mixed with the crystalline sodalite. Comparisions of the measured chemical composition to the theoretical composition to the for pure sodalite gives information on the amount of intercalated sodium hydroxide and admixed $SiO_2$ in any sample. All chemical analysis are reported on a dry weight basis to avoid confusion due to varying degrees of hydration.

Chemical Analysis

The materials used in this program were prepared by W. R. Grace Co. in two forms, oven-dried and spray-dried. After the original crystallization of the sodalite from the mother liquor, a washing step is included to remove excess uncrystallized reactants. The washed crystals are either oven- or spray-dried. In some cases, the dried crystals were leached to further reduce the amount of intercalated sodium hydroxide. A summary of the chemical composition of received material analyzed by the vendor is shown in Table B-I.

The material labeled SD-LG was orginally SD-1 which was rewashed (leached) three times to reduce the intercalated sodium hydroxide. The sodium analysis indicates that the sodium content was reduced to below the theoretical content of pure sodalite. This process has been observed in other zeolites[3] and is called decationization. Some of the cations, required to balance the charge caused by the aluminium ions in the framework, are replaced by protons.

Samples of OD-2 and SD-1 were washed in our laboratory with distilled water at 50°C for various times ranging from 12 to 72

TABLE B-I

CHEMICAL COMPOSITION OF SODALITE SAMPLES-VENDOR ANALYSIS

| Vendor Batch | ENICO Designation | % Weight, Dry Basis | | | Calculated Mole Ratios | |
|---|---|---|---|---|---|---|
| | | $Na_2O$ | $Al_2O_3$ | $SiO_4$ | Na/Al | Si/Al |
| 1 | OD-2 | 23.6[a] | 35.0[a] | 41.4[a] | 1.1 | 1.0 |
| 1 | SD-1 | 23.6[a] | 35.0[a] | 41.4[a] | 1.1 | 1.0 |
| 1 | SD-LG | 19.8 | NA[b] | NA[b] | 0.9[c] | NA[b] |

a. Values normalized to 100% from original 95.6%.

b. NA - not available.

c. Assumes no change in aluminium or silicon during leaching.

hours. These leached materials are labeled with a suffix after the basic material designation to indicate leaching and the duration. For example, oven-dried material which was leached for 48 hours is designated OD-2-L48G. The letter "G" after the letter "L" indicated that the leaching was performed by the vendor, W. R. Grace.

Two materials were prepared to test the effect of the size of the cation on krypton encapsulation and leakage properties. A sample of SD-LG was stirred in a solution of 1 M silver nitrate at 20°C for 30 minutes. The silver ions completely replaced the sodium ions in the sodalite. Potassium was used to replace sodium in a sample of SD-1 by stirring the sodalite in a 4 M potassium chloride solution at 60°C for 77 hours. The higher temperature and longer exchange time was used to enhance the exchange process, which reached 40% potassium exchange. Since the potassium ion is larger than the sodium ion, complete exchange is not feasible without major structural changes.

## Physical Properties[4]

The absolute density of the various sodalite materials was measured by helium adsorption and found to be 2.22 ± 0.5 g/cm$^3$ for eight different sodalite samples. The measured density was independent of the method of drying during the original preparation and the amount of intercalated sodium hydroxide.

The particle size of the sodalite materials was estimated from photomicrographs taken by scanning electron microscopy. Considerable agglomeration made measurement of individual crystal dimensions difficult but the average size is estimated to be on the order of several tenths of a micron ($10^{-4}$cm). The leaching process did not appear to effect the particle size.

External surface area measurements were made by the vendor on the base materials. Due to the tendency for agglomeration of the small particles, these measurements may not be representative of the specific surface of the individual sodalite crystals. The method used is the well known BET surface area method that involves adsorption of nitrogen at low temperatures. Since nitrogen is too large to enter the molecular cages, the adsorption should be only on the surface of the crystals. Agglomeration of the small crystals can create macropores in which nitrogen can be adsorbed, leading to erroneous surface area measurements.

## Crystallography

The crystal structure of sodalite has been previously determined[1,5] by X-ray diffraction studies. Analysis of various sodalite samples by X-ray powder pattern methods resulted in the following conclusions:

1. There are no detectable structural differences between oven- and spray-dried sodalites.

2. Leaching of the intercalated sodium hydroxide results in no detectable structural changes.

3. Activation (water removal) results in a slight (2%) expansion of the unit cell without significant structural change.

4. Heating sodalite above 800°C causes a drastic change in crystal structure.

5. Heating sodalite containing intercalated sodium hydroxide to 600°C under vacuum results in the formation of a significant fraction of a new phase tentatively identified as carnegieite.

6. Krypton encapsulation results in a partial unit cell contraction but no significant structural changes.

7. Potassium exchanged sodalite (40% K) shows a 3% expansion in the unit cell size but no significant structural change.

Two representative X-ray scans are shown in Figures B-2 and B-3. Figure B-2 is typical of activated sodalites and Figure B-3 shows the presence of the new phase produced by heating sodalite containing sodium hydroxide. Table B-2 summarizes the results of the X-ray analysis showing the differences between unactivated, activated, and krypton-encapsulated activated sodalite.

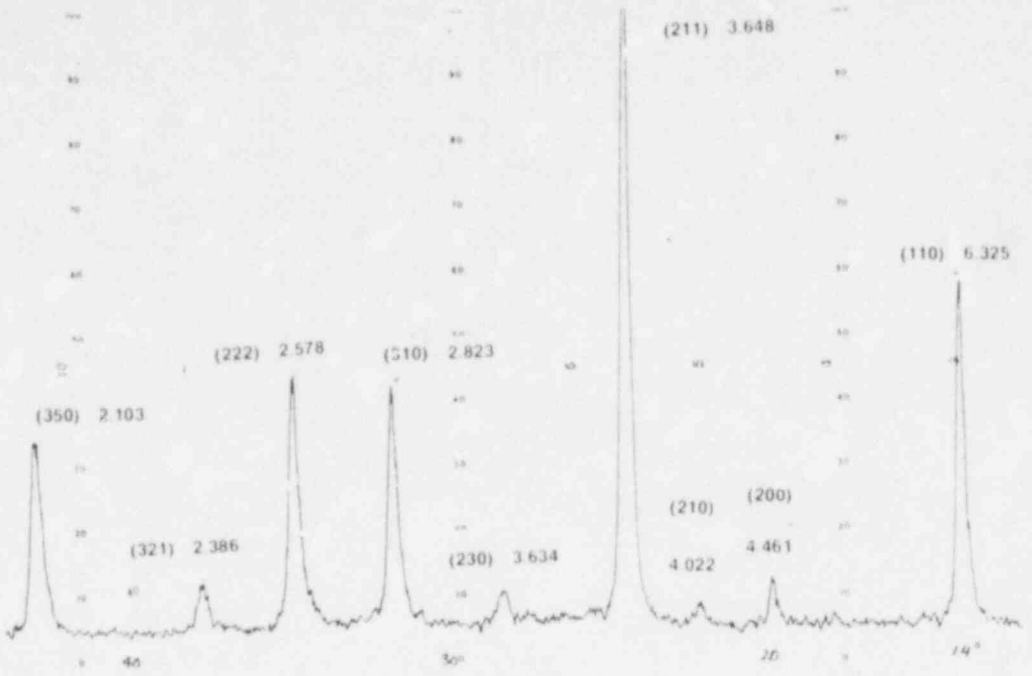


Figure B-2. Typical X-ray analysis for oven-dried sodalite activated at 400°C under vacuum.

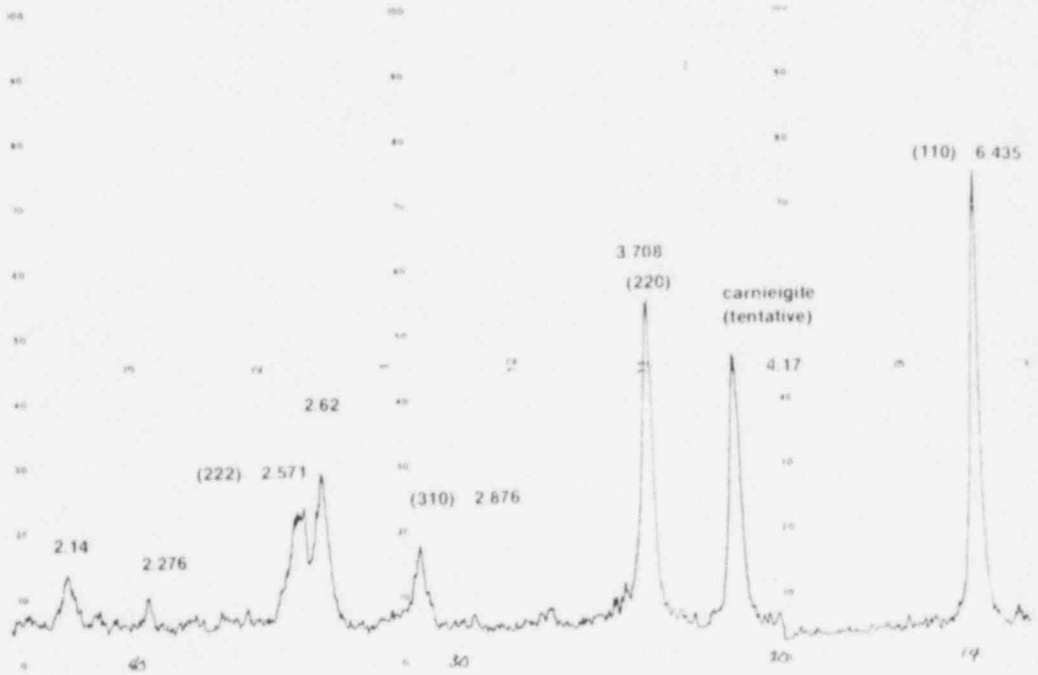


Figure B-3. X-ray analysis for oven-dried sodalite activated at 600°C under vacuum.

TABLE B-II

EFFECT OF ACTIVATION AND Kr ENCAPSULATION ON CRYSTAL STRUCTURE

| | Unactivated | | | Activated | | | Kr Encapsulated | | |
|---|---|---|---|---|---|---|---|---|---|
| | d(A) | | ao(A) | d(A) | | ao(A) | d(A) | | ao(A) |
| | (211) | (222) | | (211) | (222) | | (211) | (222) | |
| SD-1 | 3.53 | 2.57 | 8.90 | 3.69 | 2.61 | 9.03 | 3.68 | 2.62 | 9.07 |
| OD-2 | 3.64 | 2.56 | 8.86 | 3.71 | 2.62 | 9.07 | 3.69 | 2.54 | 8.79 |
| | | | | | | | | 2.61 | 9.03 |
| SD-2 | 3.64 | 2.56 | 8.86 | 3.69 | 2.60 | 9.00 | 3.69 | 2.53 | 8.75 |
| | | | | | | | | 2.61 | 9.03 |
| OD-3 | 3.63 | 2.57 | 8.90 | 3.69 | 2.62 | 9.07 | 3.70 | 2.53 | 8.75 |
| | | | | | | | | 2.60 | 9.00 |

d(a) = "d" spacing in Angstroms

Ao(A) = unit cell size in Angstroms

(211),(222) = jKL values

## REFERENCES


1. D. W. Breck, Zeolite Molecular Sieves (New York: John Wiley and Sons, 1974).

2. D. E. W. Vaughan, Encapsulation of Rare Gases, (Ph.D. Thesis, Imperial College, London, 1967).

3. R. M. Barrer, Zeolites and Clay Minerals as Sorbents and Molecular Sieves (London: Academic Press, 1978), p. 215.

4. A. B. Christensen, Physical Properties and Heat Transfer Characteristics of Materials for Krypton-85 Storage, ICP-1128 (September 1977).

5. R. M. Barrer and J. F. Cole, "Chemistry of Soil Minerals. Part VI. Salt Entrainment by Sodalite and Cancrinite During their Synthesis." J. Chem. Soc., A, 1516-1523 (1970)

DISTRIBUTION RECORD FOR ENICO-1011

Internal Distribution

1 - Chicago Patent Group - DOE
9800 South Cass
Argonne, IL 60439

1 - H. P. Pearson
Information Processing - EG&G

6 - INEL Technical Library

100 - Special Internal

External Distribution

1 - Special External

313 - UC-70 - Nuclear Waste Management

Total Copies Printed: 422